major breakthrough in establishing a biological role for RANKL-RANK interactions was the discovery that RANKL signaling through RANK is required for normal osteoclast function (22, 23). Mice deficient in either RANKL or RANK have osteopetrosis and severe skeletal abnormalities because they lack the number of osteoclasts needed to remodel bone normally. RANKL-RANK signaling is also involved in several other critical biological processes including development of lymph nodes, development of medullary thymic epithelial cells (mTEC), mammary gland lactation, and provision of survival signals to DCs (22–27). The absence of all lymph nodes in RANKL-deficient mice demonstrates that RANKL is an essential mediator in lymphoid organogenesis (22, 23). RANKL induces lymphotoxin $\alpha_1\beta_2$ expression by lymphoid tissue inducer cells in the lymph node anlage (28). RANKL is not required for PP development, but the reduced size of PP reported in two independent lines of RANKL-deficient mice indicates that RANKL contributes to normal PP development (22, 23). Functional studies of PP were not done as part of the initial characterization of these mice.

We previously showed that RANKL is selectively expressed by stromal cells in the subepithelial dome region beneath the FAE of both PP and ILF (29). Stromal cells with phenotypic characteristics similar to neonatal lymph node organizer cells including RANKL expression were recently identified in multiple secondary lymphoid tissues including mucosal-associated lymphoid tissues and lymph nodes (30). The polarized pattern of RANKL expression by stromal cells beneath the FAE of PP and ILF suggested a possible function for RANKL in regulating the induction of mucosal immune responses to particulate luminal Ags taken up through the FAE. In this study, we evaluated the function of PP in RANKL null mice and found that absence of RANKL is associated with loss of the vast majority of UEA-I$^+$ M cells in the FAE. The depletion of M cells correlated with a profound functional defect in uptake from the intestinal lumen of fluorescent beads used as model particulate Ags. Systemic administration of exogenous-soluble RANKL restored functional UEA-I$^+$ M cells to the PP of RANKL null mice and simultaneously led to widespread induction of functional M cells on the epithelium covering small intestinal villi in both RANKL null mice and wild-type mice. These findings demonstrate that the RANKL-RANK pathway plays a pivotal nonredundant role in establishing the M cell-mediated pathway of Ag acquisition and handling.

Materials and Methods

Mice

Mice carrying a RANKL null mutation on a C57BL/6 background (31) obtained from Dr. Yongwon Choi at the University of Pennsylvania (Philadelphia, PA) were used to establish a breeding colony in a conventional specific pathogen free mouse facility at Emory University. Serological sentinel testing in this facility did not include routine testing for *Helicobacter* or *Pasteurella* species, but no infections attributed to these opportunistic pathogens were demonstrated in the colony of RANKL null mice or their controls. Because RANKL null mice lack teeth, weanling null mice born in this colony are routinely given powdered mouse chow. Mice heterozygous for the RANKL null mutation were also backcrossed to BALB/c mice (Taconic Farms) for a total of four generations. Male C57BL/6 RANKL$^{+/-}$ mice and female BALB/c RANKL$^{+/-}$ mice were intercrossed to produce RANKL null mice and littermate controls on a background roughly equivalent to (C57BL/6 × BALB/c)F_1 mice. RANKL null mice on this "F_1 equivalent" genetic background are closer in weight to their heterozygous and wild-type littermates and less likely to die prematurely compared with RANKL null mice on the two inbred backgrounds. Experiments using RANKL null mice were done with mice on a C57BL/6 background mice, a (C57BL/6 × BALB/c)F_1 background, or a mixed C57BL/6 and BALB/c background, as indicated in the figure legends. BALB/c mice (Taconic Farms) were used for experiments examining induction of villous M cells by RANKL in wild-type mice and the effects of anti-RANKL mAb on PP M cells. All animal studies were reviewed and approved by the Emory University Institutional Animal Care and Use Committee.

Recombinant mouse RANKL

A bacterial expression construct encoding a glutathione S-transferase (GST) fusion protein containing amino acids 137–316 of mouse RANKL was assembled in the pGEX-5X-1 vector (GE Healthcare) using a modification of a previously described method (32). The primers 5′-CAC CCCCGGGTCAGCGCTTCTCAGGAGCT-3′ and 5′-CTCGAGTCAG TCTATGTCCTGAAC-3′ were used to PCR amplify a cDNA clone for mouse RANKL (Open Biosystems). After the PCR product was cloned into the pENTR-D-TOPO cloning vector (Invitrogen) and sequenced, the *SmaI-XhoI* fragment was subcloned into pGEX-5X-1. The construct was transformed into the BL21 *Escherichia coli* strain (Stratagene) for fusion protein expression. The cultures were induced with 20 μM IPTG for 16 h at 20°C and the GST-RANKL purified from bacterial lysate by affinity chromatography on a GSTrap FF column (GE Healthcare) followed by dialysis against multiple changes of PBS. Recombinant GST used as a control was prepared by the same method using empty pGEX-5X-1. Biological activity of the GST-RANKL fusion protein was confirmed by its ability to induce differentiation of the RAW264.7 macrophage line (American Type Culture Collection) into multinucleate osteoclasts positive for tartrate resistant acid phosphatase. The GST-RANKL fusion protein was administered to RANKL null mice by daily i.p. or s.c. injections of 50 to 250 μg per day for up to 7 days. Recombinant GST prepared from empty pGEX-5X-1 vector was used as a control for GST-RANKL.

Bacterial strains

A wild-type strain of *Salmonella enterica* serovar Typhimurium (SL3201) transformed with the DsRed-Express plasmid (Clontech) encoding a cytoplasmic red fluorescent protein was provided by Dr. Andrew Neish at Emory University (Atlanta, GA). A *Yersinia enterocolitica* isolate (ATCC 29913) was purchased from the American Type Culture Collection. For experiments involving injection of bacteria into isolated intestinal loops, these bacteria were grown overnight in LB broth, washed in PBS, and fixed in 2% paraformaldehyde for 1 h. The fixed *Yersinia* were then labeled with Alexa 546-succidymyl ester (Molecular Probes) for 1 h at room temperature following the manufacturer's suggestions.

In vivo assessment of M cell uptake of fluorescent beads and bacteria

The uptake of 200-nm diameter fluorescent polystyrene latex nanoparticles (Fluoresbrite YG; Polysciences) and fluorescent bacteria by M cells in the FAE of individual PP or by villous M cells induced by exogenous RANKL treatment was assessed by either oral gavage or by using a modification of previously described isolated small intestinal loop models (33, 34). In oral gavage experiments examining uptake of the by RANKL-induced villous M cells, aliquots of 1×10^{11} 200 nm diameter nanoparticles in a volume of 200 μl were fed to the mice. To prepare isolated small intestinal loops, mice were anesthetized using an isoflurane vaporizer. After opening the peritoneum through a longitudinal midline incision, two or three segments of small intestine measuring 2–5 cm in length and containing either a single PP (to assess PP M cell uptake) or no PP (to assess villous M cell uptake) were tied off with nylon filament. For bead uptake studies, the loops were injected with 200–400 μl of a suspension of 200 nm nanoparticles diluted in PBS to a concentration of 1×10^{11} beads/ml and returned to the peritoneal cavity. The mice were euthanized 90 to 120 min after the loops were injected, and the injected intestinal segments were excised, washed in 0.5% Tween 20-PBS, fixed in 4% paraformaldehyde in PBS for 15 min, and embedded in OCT. Frozen sections cut from these intestinal segments were examined by microscopy after counterstaining with 4′,6-diamidino-2-phenylindole (DAPI), leaving out a cold acetone fixation step because acetone dissolved the polystyrene Fluoresbrite beads, preventing their visualization. For bacterial uptake studies, loops containing no PP were injected with 300 to 500 μl of bacterial suspension at a concentration of 5×10^9 organisms/ml. After 120 min, the mice were euthanized and the intestine tissue within the loop was embedded in OCT as a Swiss roll. Frozen sections from this tissue were fixed with −20°C acetone since this fixation did not interfere with detection of the fluorescent bacteria.

Abs and lectins

mAbs for staining were purchased from eBioscience, unless otherwise stated. The mAbs used for immunofluorescence staining of frozen sections were anti-RANKL (IK22-5), anti-RANK (LOB14-8; GeneTex), PE-conjugated anti-B220 (RA3-6B2), biotinylated GL7 (for detection of activated germinal center B cells), and allophycocyanin-conjugated

anti-Thy1.2 (53-2.1; BD Biosciences). The rat mAb NKM 16-2-4 specific for mouse M cells was purified from hybridoma supernatant and labeled with FITC (35). A purified rat IgG2a isotype control mAb (BD Biosciences) was used as a control for staining of frozen tissue sections with the rat IgG2a anti-RANKL and anti-RANK mAbs. Biotinylated polyclonal goat anti-rat IgG (BD Biosciences) was used as a secondary reagent for detection of most unconjugated rat primary mAb. Rhodamine-UEA-I was purchased from Vector Laboratories. The anti-RANKL Ab (IK22-5) used for in vivo RANKL neutralization experiments was prepared as described previously (36). Mice were treated with 250 μg of IK22–5 or a purified functional grade control rat IgG2a mAb (eBioscience) i.p. every 2 days.

Immunofluorescence staining of frozen sections

Frozen sections of PP and adjacent intestinal tissue were cut on a cryostat and prepared for Ab staining experiments as previously described (29). The sections were washed in PBS and blocked in TNB buffer (PerkinElmer Life Sciences). Abs diluted in TNB buffer were applied for 1 h at room temperature or overnight at 4°C. Biotinylated primary mAbs were detected using streptavidin-conjugated peroxidase followed by FITC-tyramide from a tyramide signal amplification kit (PerkinElmer Life Sciences). Unconjugated primary rat mAbs were detected by a combination of biotinylated polyclonal goat-anti-rat IgG (BD Biosciences) followed by streptavidin-peroxidase and FITC-tyramide. DAPI (Sigma-Aldrich) at 10 ng/ml was used as a nuclear counterstain. The slides were mounted in ProLong antifade reagent (Invitrogen). Images were acquired using a Nikon 80i fluorescence microscope and edited when necessary with Photoshop (Adobe Systems).

Electron microscopy

Mice were perfusion fixed using 2.5% glutaraldehyde solution in 0.1 M cacodylate buffer. For transmission electron microscopy, individual PP were isolated, bisected through the center of the domes, and embedded in Epon resin. Thin sections from the PP domes of control and RANKL null mice were examined using a JEOL JEM-1210 microscope. For scanning electron microscopy, small intestinal villi were subjected to critical point drying, sputter coated with gold, and examined on a Topcon DS-130F field emission scanning electron microscope.

Whole mount staining of small intestine tissue for detection of UEA-I$^+$ M cells

For detection of M cells in PP, individual PP were excised and vortex mixed in 0.5% Tween 20-PBS followed by a shaking incubation with 100 μg/ml DNase for 20 min at 37°C to promote dissociation of mucus from the epithelial layer. The PP were blocked with TNB buffer for 15 min at 4°C, and stained with rhodamine-UEA-I in TNB for 40 min at 4°C. Each stained PP was mounted under a 20 mm × 20 mm coverslip in 100 μl PBS. A count of UEA-I$^+$ M cells was done for the PP follicle with the most M cells. This method resulted in some degree of underestimation of the full extent of M cell depletion in RANKL null mice because often only one of several PP follicles had any M cells in the mutant mice, while all the follicles in wild-type PP typically had a comparable number of M cells. To examine small intestine tissue for the presence of villous M cells, thin strips of tissue were cut and stained with rhodamine UEA-I as described above for PP. Villi with M cells on their surface were classified as showing a dense or diffuse pattern of villous M cells using criteria based on the initial description of these patterns by Jang et al. (9). Specifically, villi with one or more clusters of M cells in which 75% or more of the area within the cluster was occupied with M cells were considered to have a dense distribution of villous M cells. Villi with at least one characteristic UEA-I$^+$ M cell on the surface, but not meeting the dense distribution criteria, were considered to have a diffuse distribution.

Quantitative analysis of fluorescent bead and bacteria uptake by M cells

Analysis of the degree of bead uptake from loops containing PP was done by threshold analysis using ImageJ v1.36b software (http://rsb.info.nih.gov/ij/). Images of the fluorescent beads found within sections of individual PP follicles were saved as 8-bit grayscale images and then converted to binary images showing the beads by thresholding at a grayscale cutoff point of 75 of 255. The percentage of the pixels with a signal intensity that exceeded this cutoff was calculated for the area occupied by each PP follicle. Analysis of the bead uptake from loops lacking PP was done by a similar approach. Images of sections showing just the fluorescent beads within epithelial cells and the villi were thresholded at a grayscale cutoff point of 55 out of 255. Images of the DAPI-stained nuclei in the same field acquired in a separate channel were thresholded at a cutoff point of 70. The extent of bead uptake was expressed as the ratio of pixels with fluorescent beads to pixels with DAPI after normalization to a mean value of 1.0 for loops from mice not treated with RANKL. Analysis of fluorescent bacteria uptake from loops lacking PP was done by counting of the number of organisms present in sections of villi showing the villus from its base to the tip. The data were reported as the percentage of villi that included at least one organism and the average number of organisms per villus. The latter statistic was normalized to a value of 1.0 for loops from mice not treated with RANKL.

ELISA for measurement of fecal IgA

Fecal pellet samples were collected and extracted by making a 1/10 suspension (w/v) with PBS. After the suspension was vortexed and spun for 10 min at 12,000 × g, the supematant was stored at −70°C. Polyclonal goat anti-mouse IgA Ab (Southern Biotechnology) was used as a capture Ab. The bound mouse IgA was detected with peroxidase-labeled goat anti-mouse IgA Ab (Southern Biotechnology) using TMB (BD Biosciences) as the peroxidase substrate. A mouse IgA,κ isotype control mAb (BD Biosciences) was used to establish a standard curve.

Statistical analysis

Differences between the mean values for groups were analyzed by either two-tailed ANOVA with Tukey correction (for multiple groups), two-tailed Student's t test, or two-tailed Mann-Whitney U test as calculated using Prism (GraphPad Software). Differences in the frequency of bacterial uptake into villi were analyzed by Fisher's exact test and also calculated with Prism. A p-value of <0.01 was considered significant.

Results

UEA-I$^+$ M cells are dramatically decreased in the FAE of PP from RANKL null mice

M cells in mouse PP can be detected using the UEA-I lectin specific for α(1, 2)-fucose linkages. In wild-type mice, whole mount microscopy of PP follicles revealed an average of over 100 radially arranged UEA-I$^+$ M cells that extended from the edges of the follicles toward the central subepithelial dome area. In contrast, UEA-I$^+$ M cells were either completely absent or very sparsely represented in individual follicles from the PP RANKL null mice (Fig. 1*A*). The few remaining UEA-I$^+$ cells in RANKL null mice were mostly located at the periphery of the follicle and did not have the usual polygonal shape of normal M cells, features suggesting these remaining M cells were abnormal. The loss of M cells in PP from RANKL null mice was confirmed by staining PP sections with NKM 16–2-4 (supplementary Fig. S1),[4] a recently described rat mAb that is more selective than UEA-I for the specific α(1, 2)-fucose moiety characteristically displayed by mouse M cells (35). Cells with the defining ultrastructural features of M cells by transmission electron microscopy (i.e., presence of intraepithelial pockets and blunting of the apical microvilli in comparison to normal enterocytes) were readily apparent in the FAE from control mice, but absent from the FAE of RANKL null mice (Fig. 1*B*). Although the number of UEA-I$^+$ M cells was significantly decreased in all PP examined from RANKL null mice, a proximal to distal gradient in the number of UEA-I$^+$ cells per dome was observed in RANKL null mice that was not seen in wild-type mice (Fig. 1*C*). UEA-I$^+$ M cells were almost completely absent in the most proximal PP from RANKL null mice, and progressively increased in more distal PP. In RANKL null mice, the highest number of residual UEA-I$^+$ cells was consistently detected in the most distal ileal PP. Taking into account the decreases in RANKL null mice in the number of PP, the number of follicles in each PP, and the number of M cells per follicle, loss of RANKL is associated with a 73-fold overall depletion of UEA-I$^+$ M cells. This extent of loss of M cells is roughly 10-fold greater than the losses we observed in both μMT B cell deficient mice and CCR6 deficient mice

[4] The online version of this article contains supplemental material.

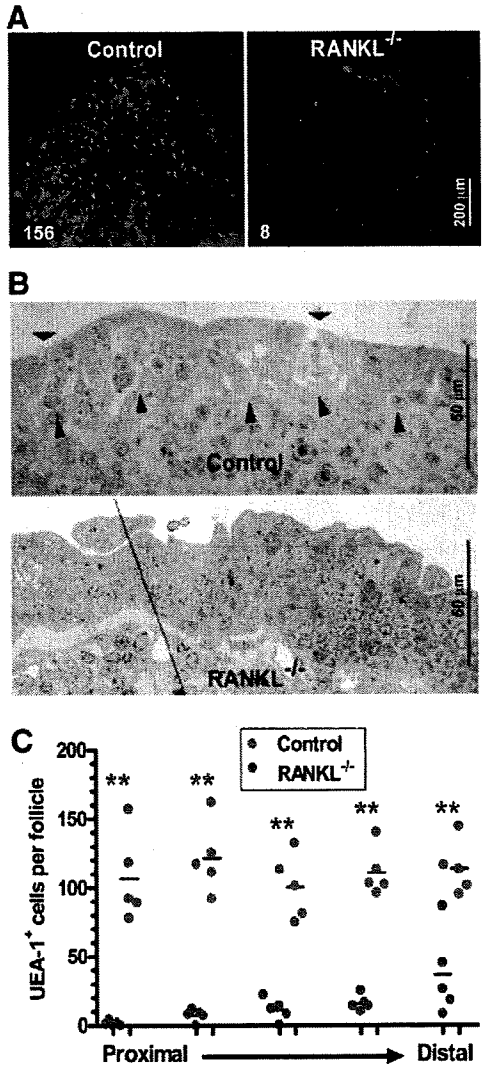

FIGURE 1. PP of RANKL null mice contain very few M cells. *A*, UEA-I staining reveals far fewer M cells in a representative follicle from a PP from a (C57BL/6 × BALB/c)F_1 RANKL null compared with a wild-type control PP. The number of M cells counted in the follicle is indicated in the lower left hand corner. The follicles shown are from the middle portion of the small intestine. Scale bar, 200 μm. *B*, FAE of a (C57BL/6 × BALB/c)F_1 RANKL null mice showed a lack of characteristic M cell features by transmission electron microscopy. The long arrowheads indicate intraepithelial pockets within the M cells of the wild-type FAE. The short arrowheads point to the shorter microvilli found on the apical surface of M cells. Scale bars, 50 μm. *C*, Scatter plot summarizing frequency of UEA-I^+ M cells in individual PP follicles from mixed background RANKL null and control mice (n = 5 mice for both groups). All PP examined were assigned to 1 of 5 groups based on proximal to distal position. **, $p \leq 0.001$ compared with control mice by ANOVA.

(data not shown), strains of mutant mice previously shown to have a significant reduction in the number of M cells (37, 38).

UEA-I^+ M cells can be restored in RANKL null mice by treatment with exogenous RANKL

To determine whether the deficiency of M cells in the FAE of RANKL null PP could be restored by replacement of RANKL, RANKL null mice were injected i.p. for 7 consecutive days with 250 μg per day of either recombinant GST-RANKL fusion protein or recombinant GST as a control. On day 7, the PP follicles of RANKL null mice treated with GST-RANKL had a near normal number of UEA-I^+ M cells distributed in the typical radial pattern, while GST-treated mice remained profoundly M cell deficient (Fig. 2*A*). Daily treatment of RANKL null mice with rGST-RANKL for shorter intervals demonstrated that day 5 was the first time point at which the number of UEA-I^+ M cells was significantly increased over untreated RANKL null mice (Fig. 2*B*).

RANKL null mice have a defect in the uptake of 200 nm fluorescent beads into PP follicles that is corrected by administration of RANKL

Although UEA-I is a useful immunohistochemical marker of mouse M cells, this method of identification does not detect M cells based on their specialized ability to take up particulate Ags from the lumen and transport them to meet APC in the intraepithelial pockets. Measuring uptake of fluorescent nanoparticles injected into loops of small intestine is a method that directly assesses M cell function in the FAE of PP (33, 34). Frozen sections of PP in isolated loops of small intestine from RANKL null mice and RANKL null mice treated with GST-RANKL or GST (as a control) were compared at 90 min after injection of fluorescent 200 nm nanoparticles into the loops. In the GST-RANKL-treated mice, more UEA-I^+ M cells were present and some of these cells contained multiple fluorescent beads (Fig. 2*C*). Beads that had already passed through the epithelial layer to reach the PP follicle were observed in APC in the vicinity of the subepithelial dome or deeper in the B cell follicle. Image analysis was used to quantify the magnitude of bead uptake in the GST-RANKL reconstituted mice and controls (Fig. 2*D*). Untreated RANKL null mice or those treated with GST had over 10-fold less uptake of beads than control wild-type mice. GST-RANKL treatment for 7 days restored bead uptake to near wild-type levels.

Systemic administration of RANKL also leads to widespread induction of villous M cells

In the course of treating RANKL null mice with GST-RANKL and evaluating the reconstitution of M cells in PP, we noticed that the number of UEA-I^+ cells present on small intestinal villi was also increased. This effect of RANKL treatment was further evaluated in BALB/c mice, in which <10% of small intestinal villi have any villous M cells at baseline, with most of these rare villous M cells arranged in a diffuse pattern. Treatment with systemic GST-RANKL i.p. for 4 consecutive days induced substantial increase in the number of UEA-I^+ cells with the features of M cells on the surface of the villi (Fig. 3*A*). Induction of an increased number of villous M cells began by 24 h after the first injection of GST-RANKL; 4 days after the start of RANKL treatment all small intestinal villi had at least some UEA-I^+ cells present, with 70% of villi showing a diffuse pattern and the remaining 30% exhibiting a dense pattern (Fig. 3*B*). In villi showing a diffuse pattern of villous M cells, UEA-I^+ cells represented ~3% of the total number of cells with $DAPI^+$ nuclei. Scanning electron microscopy of villi from RANKL-treated mice revealed slightly sunken cells with the characteristic stubby microvilli characteristic of M cells (Fig. 3*C*).

RANKL-induced villous M cells are functional M cells capable of taking up 200 nm beads and enteric bacteria

To determine whether the villous M cells induced by systemic RANKL treatment were capable of increased transport of particulate Ags across the epithelium, mice were treated with s.c. injections of GST-RANKL or GST as a control for 4 consecutive days and gavaged with 200 nm diameter fluorescent nanoparticles at the same time as the last two RANKL injections. Small intestinal segments from these mice were excised 24 h after the second dose of beads and frozen sections cut to identify beads that had been taken

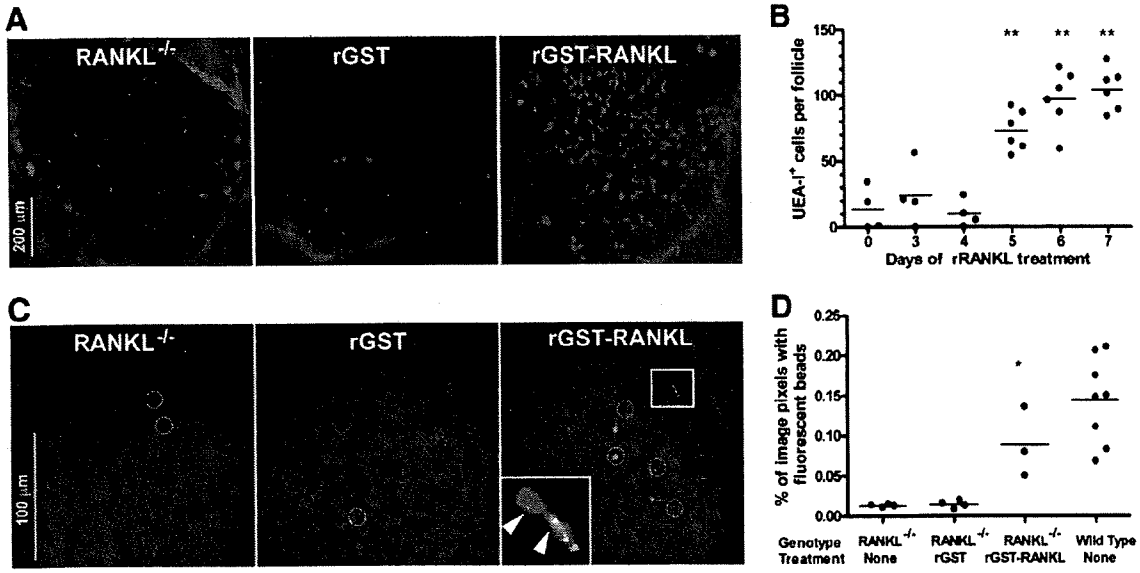

FIGURE 2. Administration of rRANKL to RANKL null mice restores PP M cells. *A*, (C57BL/6 × BALB/c)F_1 RANKL null mice were treated i.p. for 7 days with 250 μg/day of GST-RANKL or GST as a control. UEA-I staining of representative follicles from the distal small intestine shows restoration of the normal number and pattern of UEA-I^+ M cells by GST-RANKL, but not by GST. Scale bar, 200 μm. *B*, Reconstitution of UEA-I^+ M cells requires 5 days of treatment with GST-RANKL. The results are based on three to six mixed background mice at each time point and include data from all PP except the most distal PP. **, $p \leq 0.001$ compared with untreated mice by ANOVA. *C*, Uptake of 200-nm diameter fluorescent beads from isolated small intestinal loops into PP of mixed background RANKL null mice 90 min after bead injection is restored to near wild-type levels by prior treatment with GST-RANKL for 5 days. Merged images of bead fluorescence and DAPI fluorescence from frozen sections of PP are shown with the white circles indicating the location of individual beads or clusters of beads. The inset shows a magnified image of the boxed area additionally merged with the rhodamine-UEA-I signal to show that the clusters of fluorescent beads (indicated by arrowheads) within two adjacent UEA-I^+ M cells on the surface of the FAE. Scale bar, 100 μm. *D*, Summary scatter plot showing that GST-RANKL treatment reconstitutes uptake of fluorescent beads as assessed by image analysis of the percentage of pixels containing green fluorescent beads within the area of the PP follicles. *, $p < 0.01$ compared with untreated RANKL-null mice by ANOVA.

up into the lamina propria by M cells. Bead uptake was readily apparent in M cells and within the villi of the RANKL-treated mice, but barely evident in the control untreated mice (Fig. 4*A*). Uptake of fluorescent beads was increased by an average of 74-fold over the baseline of untreated mice as a result of RANKL-induction of villous M cells (Fig. 4*B*). To test whether the RANKL-induced villous M cells were also capable of enhanced uptake of enteric bacteria, isolated segments of small intestine lacking any PP from mice treated with GST-RANKL or GST for 4 days were injected with fluorescently labeled paraformaldehyde-fixed enteric bacteria. Sections of the intestinal wall taken 2 h after the introduction of the bacteria revealed substantially enhanced uptake of both *Salmonella enterica* serovar Typhimurium (35-fold) and *Yersinia enterocolitica* (46-fold) as a consequence of villous M cell induction by RANKL (Fig. 4, *C* and *D*).

Neutralizing Ab to RANKL reproduces the M cell deficiency observed in RANKL null mice

Some of the developmental defects in RANKL null mice, such as the total absence of lymph nodes, cannot be corrected by simply injecting the mice with the absent cytokine as adults. This raises the issue of whether the M cell deficit observed in PP from RANKL null mice might be a byproduct of early developmental alterations in the PP of these mice. To address this issue, wild-type BALB/c mice were treated i.p. with a neutralizing anti-RANKL Ab to determine whether acute blockade of RANKL-RANK signaling would lead to loss of PP M cells. Mice were treated i.p. with 250 μg of the IK22–5 rat anti-mouse RANKL mAb every 2 days, a dose previously shown to block the activity of RANKL in vivo (36). The number of M cells in the PP follicles was evaluated after various lengths of treatment by both UEA-I staining and by uptake of fluorescent 200 nm beads from isolated small intestinal loops. After 8 days of Ab treatment, the number of M cells present in the PP and the degree of uptake of fluorescent beads by PP in isolated loops were both dramatically decreased compared with untreated mice or mice treated with an isotype control IgG2a mAb (Fig. 5, *A–C*). Analysis of the kinetics of the anti-RANKL effects showed that the number of UEA-I^+ M cells dropped precipitously between 2 and 4 days, and declined further between 4 and 8 days (Fig. 5*D*).

Epithelial cells in the small intestine express RANK

RANK is expressed by multiple cell types including osteoclasts, DCs, mammary epithelial cells, and thymic epithelial cells. Because our experiments with RANKL null mice and neutralizing anti-RANKL Ab showed that RANKL is essential for normal M cell development within the FAE, we used immunohistochemical staining with anti-RANK Abs to determine what cells in the vicinity of PP expressed the RANK. Staining for RANK was observed on the apical and basolateral aspects of epithelial cells in the FAE, and was also detected on villous and crypt epithelial cells (Fig. 6). Serial sections of the same PP showed that RANKL expression was restricted to stromal cells concentrated beneath the FAE as previously shown (29). These results suggest that RANKL exerts its effects on M cell differentiation through short-range delivery from the stromal cells to the FAE on the other side of the basement membrane.

RANKL null mice exhibit decreased PP germinal center formation and fecal IgA production

PP were previously reported to be smaller than normal in two independently derived strains of RANKL null mice (22, 23), but other aspects of PP function were not examined in the initial reports. We asked whether the loss of M cell function in RANKL null mice was associated with impaired B cell responses to Ags

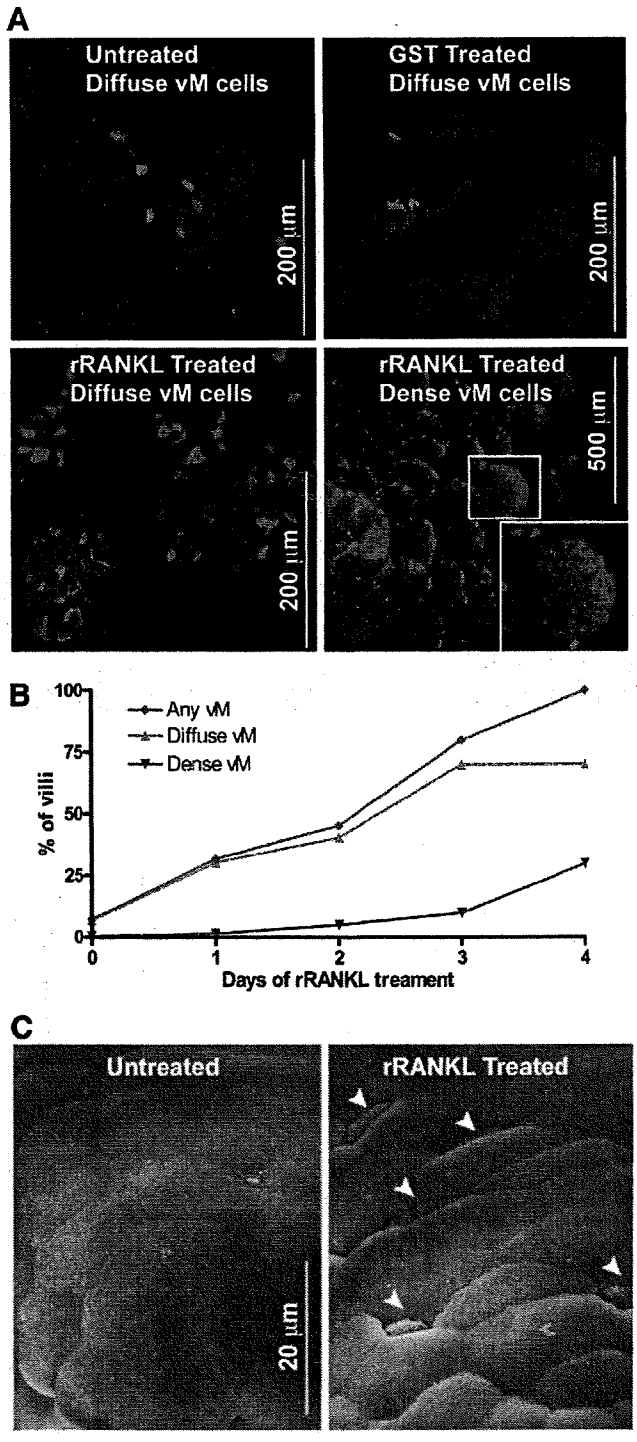

FIGURE 3. Administration of rRANKL induces development of villous M cells on all small intestinal villi. *A*, Whole mount staining of villous M cells in untreated BALB/c mice and mice treated for 4 days with GST-RANKL or GST (an initial injection of 50 μg i.p. followed by 100 μg s.c. every 24 h) with rhodamine-UEA-I and DAPI. In untreated mice, a few villous M cells in a diffuse pattern are present on occasional villi. GST-RANKL treatment leads to an increased fraction of the villi having M cells and an increase in the number of M cells per villus. The fraction of villi exhibiting both the diffuse and dense patterns of villous M cell distribution increases after GST-RANKL. Scale bars, 200 μm and 500 μm. *B*, Summary graph showing kinetics of induction of villous M cells in the diffuse and dense patterns of distribution following GST-RANKL administration. *C*, Scanning electron microscopy reveals the presence of cells with a depressed surface and attenuated and blunted microvilli characteristic of M cells.

internalized from the intestinal lumen. We compared the frequency and extent of germinal center development in PP from RANKL null mice and littermate controls using an Ab (GL7) that preferentially binds activated germinal center B cells. Compared with PP from controls, PP from RANKL null mice at 10 to 12 wk of age exhibited a smaller percentage of germinal centers containing $GL7^+$ cells in the B cell zones and a relative expansion of the T cell zones (Fig. 7*A*). This finding suggested that the production of secretory IgA might also be impaired in RANKL null mice. Fecal IgA concentrations in mice from 4 to 12 wk of age were consistently decreased in RANKL null mice compared with littermate controls (Fig. 7*B*).

Discussion

Ag-sampling M cells have been described in both mammalian and avian species as part of the FAE covering the organized lymphoid structures of the respiratory and digestive tract (3, 39, 40). However, the specific signals and signaling pathways that trigger the differentiation of these M cells from precursor cells located in the stem cell zone of the crypts or from the enterocytes on the surface of the FAE remain to be identified (12). Some clues have emerged from analysis of strains of mutant mice created by gene-targeting that retain PP but exhibit decreased numbers of M cells in these PP. Specifically, B cell-deficient mice such as μMT mice exhibit significantly reduced numbers of M cells in PP (37). Additional support for a role of B cells in promoting M cell development has come from in vitro studies in which coculture of freshly isolated B lymphocyte or B lymphocyte lines with model intestinal epithelial cell lines cultured on semipermeable supports promoted the development of M cell-like features by the epithelial cells, including transcytosis of particulate Ags (11, 41). However, neither in vivo analysis of PP from B cell-deficient mice or experiments based on the in vitro M cell differentiation system have elucidated a specific mechanism by which B cells promote differentiation of M cells in the FAE.

RANKL emerged as a cytokine with a potential role in the differentiation of the FAE and M cells as a result of experiments demonstrating RANKL expression on stromal cells located immediately beneath the FAE in ILF and PP (29). To determine whether PP were functionally compromised in the absence of RANKL, we characterized the PP of RANKL null mice. Staining of PP from RANKL null mice with the UEA-I lectin reactive with murine M cells revealed a profound depletion in $UEA\text{-}I^+$ cells compared with wild-type mice. Taking into account all of the factors that contribute to the total number of M cells within small intestinal PP (i.e., number of PP, number of follicles per PP, number of M cells per follicle), we found that RANKL null mice have <2% of the number of $UEA\text{-}I^+$ M cells found in wild-type mice. Although the UEA-I lectin was the primary immunohistochemical reagent we used to establish that RANKL null mice are deficient in M cells, we have used several independent means of confirming this deficiency in M cells including functional measurements of M cell activity using uptake of fluorescent nanoparticles and bacteria, transmission electron microscopy, and immunostaining with the NKM 16–2-4 mAb specific for mouse M cells.

RANKL acting through its specific receptor (RANK) plays an important developmental role in multiple tissues. The most striking and best-studied of the deficits in RANKL null mice are the absence of any lymph nodes and the failure of osteoclast development, leading to osteopetrosis and a malformed skeleton. One potential explanation of the loss of M cells we observed in PP from RANKL null mice is an early developmental defect in PP development that permanently compromises the capacity of the FAE to generate conventional M cells. Two types of experiments were

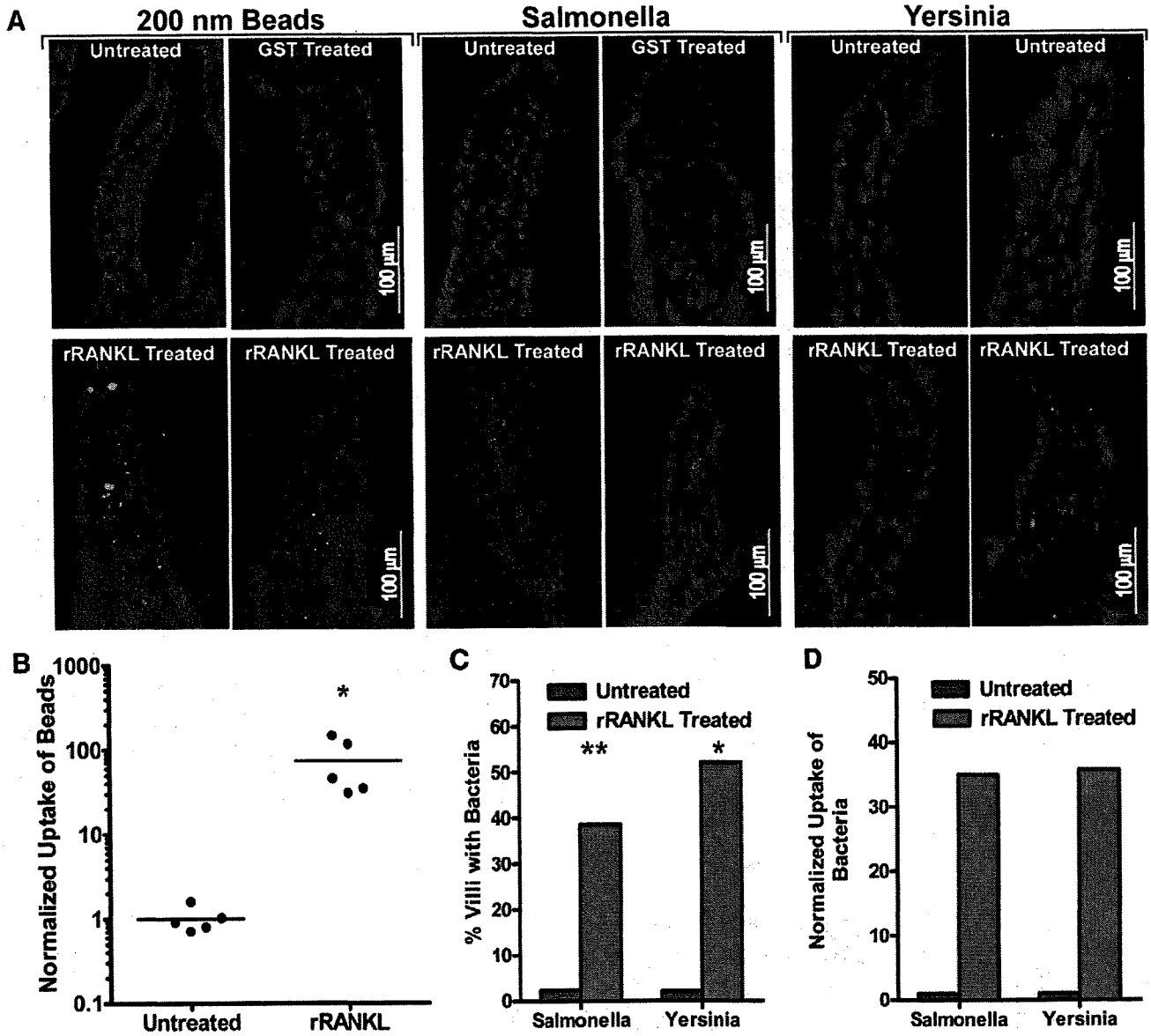

FIGURE 4. RANKL-induced villous M cells are functional for bead and bacteria uptake from the intestinal lumen. *A*, Wild-type (C57BL/6 × BALB/c)F_1 mice were treated with 100 μg of GST-RANKL or GST s.c. once a day for 4 consecutive days. On the last two days of injections, the mice and untreated controls also received 1×10^{11} 200 nm fluorescent beads by gavage. One day after the last dose of GST-RANKL or GST, segments of small intestine were harvested and sectioned to check for the presence of green fluorescent beads. Alternatively, isolated small intestinal loops were prepared in anesthetized mice treated for 4 days with RANKL or GST and untreated controls and these loops were injected with paraformaldehyde-fixed *Salmonella enterica* serovar Typhimurium expressing DsRed-Express or *Yersinia enterocolitica* labeled with Alexa546. After a 2-h incubation, the tissue was harvested for frozen sections. The merged images show representative villi with DAPI-positive nuclei and either green fluorescent beads or red fluorescent bacteria within the villi. *B*, Uptake of beads was quantitated by image analysis and normalized so that the average uptake in untreated controls was 1.0. *, $p < 0.01$ by Mann-Whitney *U* test. *C*, The percentage of villi containing at least one bacterial organism was substantially increased in RANKL-treated mice. **, $p \leq 0.001$; *, $p < 0.01$ (both by Fisher's exact test). *D*, Uptake of bacteria was quantitated by counting individual bacteria within villi. The mean number of bacteria found per villus was normalized to a value of 1.0 for the untreated controls.

done to test this possibility. First, we examined whether the M cell defect was reversible if a source of exogenous recombinant RANKL was provided. Daily injections of GST-RANKL given for 5 or more days provided a nearly complete reconstitution of the number of M cells per PP follicle. Second, we used neutralizing mAb to RANKL to test whether acute depletion of RANKL in adult wild-type mice would also cause loss of M cells. After 4 days of anti-RANKL treatment to inhibit normal RANKL-RANK interactions, the number of UEA-I^+ M cells in each PP follicle plunged to levels approaching those in the RANKL null mice. Thus, production of RANKL must be sustained in the adult PP to permit the continued production and/or survival of M cells.

RANK is expressed on multiple cell types including osteoclasts and their precursors, DCs, endothelial cells, mTEC, and mammary epithelial cells. The simplest model to explain the observed effects of RANKL on M cell differentiation is to propose that RANKL derived from the subepithelial dome stromal cells in the PP acts in a paracrine fashion on the adjacent epithelial cells of the FAE. Because RANKL is a type II membrane protein that is synthesized in a transmembrane form, cleavage by metalloproteases is needed

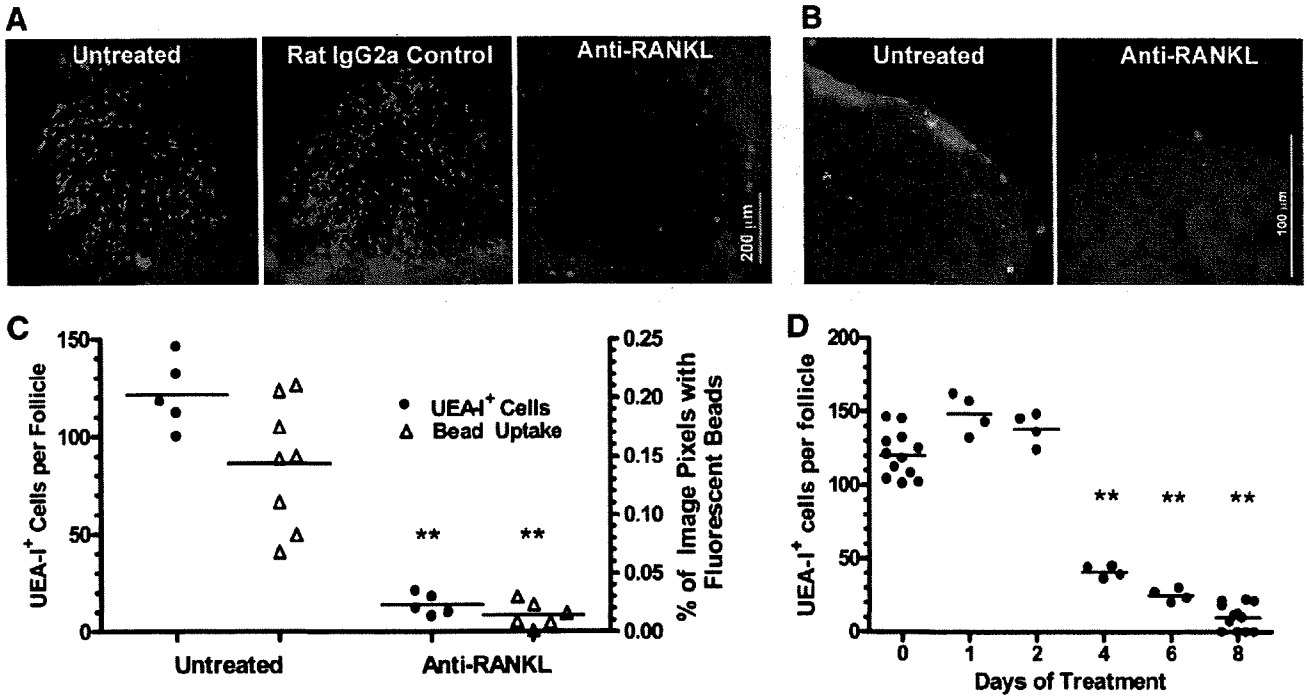

FIGURE 5. Treatment of wild-type mice with neutralizing anti-RANKL leads to loss of PP M cells. *A* and *B*, BALB/c mice were treated i.p. with 250 μg of IKK22–5 mAb or an isotype control rat IgG2a mAb on days 0, 2, 4, and 6. On day 8, isolated bowel loops containing PP were injected with fluorescent beads and the mice euthanized after 90 min. Anti-RANKL treatment led to loss of UEA-I$^+$ M cells detected by whole mount staining (*A*) and a decrease in the uptake of fluorescent beads detected on frozen sections of PP from the bead-injected loops (*B*). Scale bar, 200 μm in *A* and 100 μm in *B*. *C*, Summary of data from all PP analyzed in *A* and *B* for UEA-I$^+$ cells and fluorescent bead uptake. *D*, Anti-RANKL-induced loss of UEA-I$^+$ M cells detected by whole mount staining begins by 4 days after start of Ab treatment. ** in *C* and *D* indicates $p < 0.001$ compared with untreated mice by *t* test (*C*) or ANOVA (*D*).

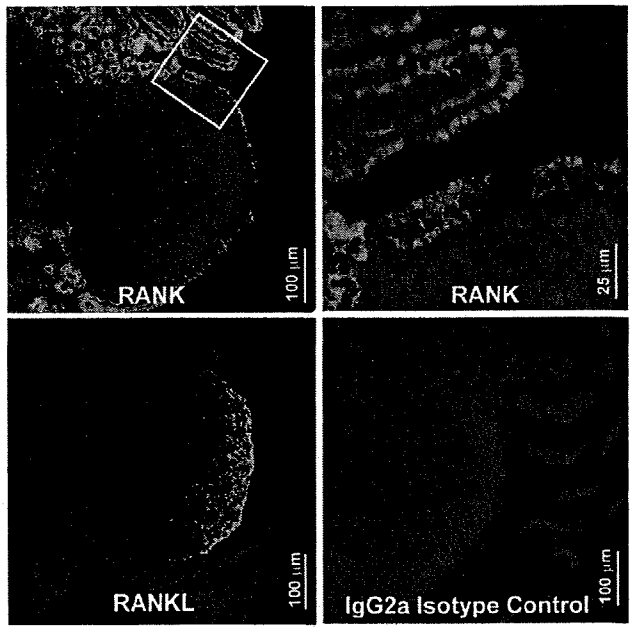

FIGURE 6. Intestinal epithelial cells express RANK. Frozen sections of a PP from a single wild-type BALB/c mouse were stained with rat mAbs to mouse RANK (*A* and *B*), mouse RANKL (*C*), or an isotype control rat IgG2a mAb (*D*), followed by a biotinylated secondary Ab, streptavidin-peroxidase, and FITC-tyramide plus DAPI as a counterstain. *A*, RANK expression is localized to epithelial cells in the FAE and on the adjacent villi. Scale bar, 100 μm. *B*, Higher magnification of boxed area from *A* showing that RANK is present on both the apical and basolateral surfaces of the FAE. Scale bar, 250 μm. *C*, Reticular stromal cells concentrated immediately beneath the epithelial layer are the only cells on which RANKL is detected. Scale bar, 200 μm. *D*, No staining is observed with the rat IgG2a isotype control.

to generate a soluble form of the cytokine (17, 18). We favor the hypothesis that RANKL is acting directly through RANK on enterocytes because immunohistochemical staining of small intestinal tissue including a PP showed that the bulk of the RANK staining is localized to the epithelium, with roughly equivalent levels of RANK on the FAE and villous epithelium. Gene expression profiling studies comparing flow sorted PP M cells and villous enterocytes revealed that both of these intestinal epithelial cell types express mRNA for RANK (35) (gene expression data for RANK archived in NCBI Gene Expression Omnibus under accession number GSE7838; http://www.ncbi.nlm.nih.gov/geo/query/acc.cgi?acc=GSE7838). Although the induction of M cells by RANKL appears to be mediated by direct action of RANKL on RANK-expressing epithelial cells, other cell types in the small intestine are known to express RANK and respond to RANKL. For example, RANKL was shown to act on PP DC to enhance IL-10 production (42). In addition, Ab-mediated neutralization of RANKL in a transfer model of colitis resulted in decreased regulatory T cell activity, suggesting that RANKL-RANK signaling contributes to the normal function of regulatory T cells (43).

The capacity of soluble recombinant RANKL injected systemically to induce the appearance of M cells on all small intestinal villi provides further insights into the mechanism of action of RANKL. RANK-expressing epithelial precursor cells located in both dome-associated crypts next to PP follicles and in standard small intestinal crypts have the potential to differentiate into M cells if exposed to sufficient stimulation with RANKL. RANKL-induced villous M cells have most of the same features as PP M cells, including reactivity with UEA-I, stubby surface microvilli observed by scanning electron microscopy, and most importantly the capacity for constitutive uptake of particulate Ags. Under normal conditions, M cell development is primarily restricted (other than a small number of scattered villous M cells) to the organized

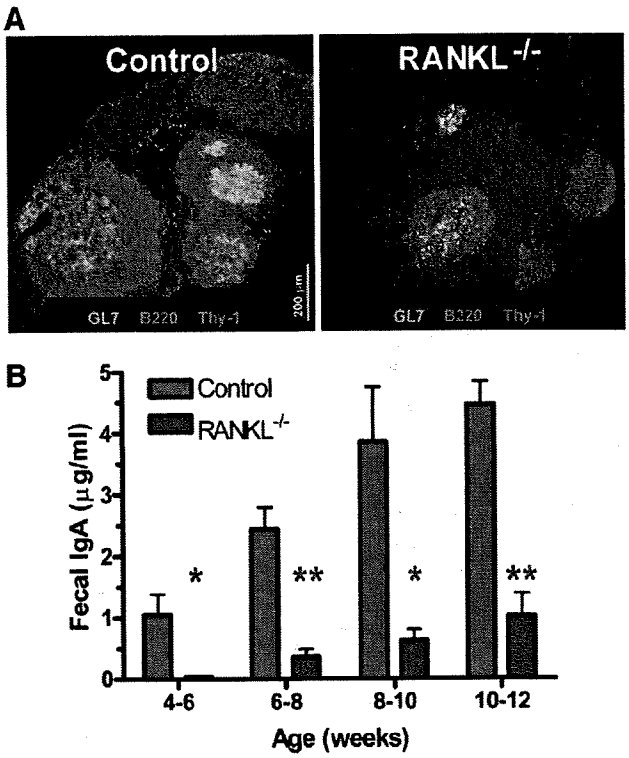

FIGURE 7. RANKL$^{-/-}$ mice have fewer germinal centers in their PP follicles and lower levels of fecal IgA. *A*, RANKL$^{-/-}$ PP on a mixed C57BL/6 and BALB/c background have fewer and less developed germinal centers identified by GL7$^+$ cells than control PP. *B*, Fecal IgA concentrations (mean ± SD) measured by ELISA were consistently decreased in RANKL$^{-/-}$ mice compared with littermate controls based on analysis of samples from 5 to 16 mice of each genotype in each age range tested. *, $p < 0.01$; **, $p < 0.001$ (compared with control mice by *t* test).

lymphoid tissues of the small intestine (i.e., PP and ILF) because constitutive expression of RANKL is restricted to subepithelial stromal cells at these sites. When the spatial restriction of RANKL availability in the small intestine is bypassed by systemic injection, RANKL is able to trigger M cell differentiation in a fraction of epithelial precursors in both dome-associated crypts adjacent to organized lymphoid tissues and normal crypts.

Although our results identify RANKL as a key cytokine signal involved in inducing the differentiation of M cells from precursors in the FAE, we consistently observed a trace number of residual UEA-I$^+$ M cells in a few of the PP follicles in RANKL null mice. Our results fit best with a model that postulates that there are additional signals besides RANKL that contribute to the development of M cells. We found that the most distal PP in RANKL null mice was invariably the PP with the largest number of residual M cells per follicle, suggesting that an increased density of luminal commensal bacteria can accentuate the extent of M cell differentiation locally in situations in which loss of an M cell-inducing factor results in a global decrease in M cell differentiation. One of the other signals capable of promoting M cell development may be contributed by local B cells in the PP, because absence of mature B cells also leads to depletion of PP M cells (37), although the degree of M cell deficit is far less pronounced. Exogenous administration of GST-RANKL to B cell deficient $J_H^{-/-}$ mice does not increase the number of PP M cells (our unpublished observations), indicating that the contribution of B cells to the development of M cells does not involve simply providing RANKL. Given that TNF family members are known to have overlapping and partially redundant functions in other developmental contexts (e.g., the known contributions of lymphotoxin $\alpha_1\beta_2$, RANKL, and TNF-α to the normal formation and organization of secondary lymphoid structures) (44), other TNF family members may contribute to the induction of M cell differentiation and account for the low level of residual M cell formation in the absence of RANKL. Cooperation of RANKL with the TNF family member CD40L has recently been established for the induction of mTEC differentiation (24, 25). RANKL is the most critical TNF family member in inducing normal mTEC differentiation during embryonic development of the thymus, with CD40L playing a complementary role in the postnatal thymus (24). Interesting parallels exist between the role of RANKL in inducing differentiation of UEA-I$^+$ M cells in the FAE of PP and its role in inducing the differentiation of UEA-I$^+$ mTEC in the thymus. The RANKL-induced mTECs are critical for establishment of central T cell tolerance, while RANKL-induced M cells contribute to the establishment of peripheral T cell tolerance to bacterial Ags at mucosal surfaces normally colonized by commensal bacteria.

The identification of RANKL as a key switch factor that can elicit M cell development by intestinal epithelial precursors has the potential to yield valuable translational applications in the areas of mucosal vaccine development and oral tolerance induction. Specifically targeting orally administered Ags to M cells using either mAbs to M cell surface receptors, lectins, or bacterial adhesins specific for M cells remains an active area in the development of vaccines for oral delivery (45, 46). Combining Ab-mediated M cell targeting of Ag with a strong mucosal adjuvant (e.g., cholera toxin) already shows promise as a strategy for the establishment of both mucosal and systemic immunity to vaccine Ags (47). The efficacy of such approaches may be boosted if preceded by systemic or ideally local delivery of exogenous RANKL aimed at increasing the frequency of human M cells in the PP FAE and particularly in the villous epithelium to supraphysiologic levels, thereby increasing the efficiency of delivery of M cell-targeted vaccines administered at mucosal surfaces.

Acknowledgments

We thank Dr. Max Cooper for valuable suggestions and Dr. Tim Denning for comments on the manuscript. We also thank Dr. Yongwon Choi for providing us with RANKL knockout mice, Katy Gray in Dr. Sam Speck's laboratory for help obtaining breeder pairs of µMT mice, and Jeannette Taylor from the Robert P. Apkarian Integrated Electron Microscopy Core for expert technical assistance with electron microscopy.

Disclosures

The authors have no financial conflict of interest.

References

1. Fagarasan, S., and T. Honjo. 2004. Regulation of IgA synthesis at mucosal surfaces. *Curr. Opin. Immunol.* 16: 277–283.
2. Iweala, O. I., and C. R. Nagler. 2006. Immune privilege in the gut: the establishment and maintenance of non-responsiveness to dietary antigens and commensal flora. *Immunol. Rev.* 213: 82–100.
3. Kraehenbuhl, J. P., and M. R. Neutra. 2000. Epithelial M cells: differentiation and function. *Annu. Rev. Cell Dev. Biol.* 16: 301–332.
4. Pabst, O., G. Bernhardt, and R. Forster. 2007. The impact of cell-bound antigen transport on mucosal tolerance induction. *J. Leukocyte Biol.* 82: 795–800.
5. Martinoli, C., A. Chiavelli, and M. Rescigno. 2007. Entry route of *Salmonella typhimurium* directs the type of induced immune response. *Immunity* 27: 975–984.
6. Hashizume, T., A. Togawa, T. Nochi, O. Igarashi, M. N. Kweon, H. Kiyono, and M. Yamamoto. 2008. Peyer's patches are required for intestinal immunoglobulin A responses to *Salmonella*. *Infect. Immun.* 76: 927–934.
7. Macpherson, A. J., and T. Uhr. 2004. Compartmentalization of the mucosal immune responses to commensal intestinal bacteria. *Ann. NY Acad. Sci.* 1029: 36–43.
8. Suzuki, H., S. Sekine, K. Kataoka, D. W. Pascual, M. Maddaloni, R. Kobayashi, K. Fujihashi, H. Kozono, J. R. McGhee, and K. Fujihashi. 2008. Ovalbumin-protein sigma 1 M-cell targeting facilitates oral tolerance with reduction of antigen-specific CD4$^+$ T cells. *Gastroenterology* 135: 917–925.

9. Jang, M. H., M. N. Kweon, K. Iwatani, M. Yamamoto, K. Terahara, C. Sasakawa, T. Suzuki, T. Nochi, Y. Yokota, P. D. Rennert, et al. 2004. Intestinal villous M cells: an antigen entry site in the mucosal epithelium. *Proc. Natl. Acad. Sci. USA* 101: 6110–6115.
10. Owen, R. L., and A. L. Jones. 1974. Epithelial cell specialization within human Peyer's patches: an ultrastructural study of intestinal lymphoid follicles. *Gastroenterology* 66: 189–203.
11. Kerneis, S., A. Bogdanova, J. P. Kraehenbuhl, and E. Pringault. 1997. Conversion by Peyer's patch lymphocytes of human enterocytes into M cells that transport bacteria. *Science* 277: 949–952.
12. Mach, J., T. Hshieh, D. Hsieh, N. Grubbs, and A. Chervonsky. 2005. Development of intestinal M cells. *Immunol. Rev.* 206: 177–189.
13. Kerneis, S., and E. Pringault. 1999. Plasticity of the gastrointestinal epithelium: the M cell paradigm and opportunism of pathogenic microorganisms. *Semin. Immunol.* 11: 205–215.
14. Gebert, A., S. Fassbender, K. Werner, and A. Weissferdt. 1999. The development of M cells in Peyer's patches is restricted to specialized dome-associated crypts. *Am. J. Pathol.* 154: 1573–1582.
15. Lelouard, H., A. Sahuquet, H. Reggio, and P. Montcourrier. 2001. Rabbit M cells and dome enterocytes are distinct cell lineages. *J. Cell Sci.* 114: 2077–2083.
16. Bachmann, M. F., B. R. Wong, R. Josien, R. M. Steinman, A. Oxenius, and Y. Choi. 1999. TRANCE, a tumor necrosis factor family member critical for CD40 ligand-independent T helper cell activation. *J. Exp. Med.* 189: 1025–1031.
17. Lum, L., B. R. Wong, R. Josien, J. D. Becherer, H. Erdjument-Bromage, J. Schlondorff, P. Tempst, Y. Choi, and C. P. Blobel. 1999. Evidence for a role of a tumor necrosis factor-α (TNF-α)-converting enzyme-like protease in shedding of TRANCE, a TNF family member involved in osteoclastogenesis and dendritic cell survival. *J. Biol. Chem.* 274: 13613–13618.
18. Hikita, A., I. Yana, H. Wakeyama, M. Nakamura, Y. Kadono, Y. Oshima, K. Nakamura, M. Seiki, and S. Tanaka. 2006. Negative regulation of osteoclastogenesis by ectodomain shedding of receptor activator of NF-κB ligand. *J. Biol. Chem.* 281: 36846–36855.
19. Wong, B. R., R. Josien, S. Y. Lee, M. Vologodskaia, R. M. Steinman, and Y. Choi. 1998. The TRAF family of signal transducers mediates NF-κB activation by the TRANCE receptor. *J. Biol. Chem.* 273: 28355–28359.
20. Galibert, L., M. E. Tometsko, D. M. Anderson, D. Cosman, and W. C. Dougall. 1998. The involvement of multiple tumor necrosis factor receptor (TNFR)-associated factors in the signaling mechanisms of receptor activator of NF-κB, a member of the TNFR superfamily. *J. Biol. Chem.* 273: 34120–34127.
21. Simonet, W. S., D. L. Lacey, C. R. Dunstan, M. Kelley, M. S. Chang, R. Luthy, H. Q. Nguyen, S. Wooden, L. Bennett, T. Boone, et al. 1997. Osteoprotegerin: a novel secreted protein involved in the regulation of bone density. *Cell* 89: 309–319.
22. Kong, Y. Y., H. Yoshida, I. Sarosi, H. L. Tan, E. Timms, C. Capparelli, S. Morony, A. J. Oliveira-dos-Santos, G. Van, A. Itie, et al. 1999. OPGL is a key regulator of osteoclastogenesis, lymphocyte development and lymph-node organogenesis. *Nature* 397: 315–323.
23. Kim, N., P. R. Odgren, D. K. Kim, S. C. Marks, Jr., and Y. Choi. 2000. Diverse roles of the tumor necrosis factor family member TRANCE in skeletal physiology revealed by TRANCE deficiency and partial rescue by a lymphocyte-expressed TRANCE transgene. *Proc. Natl. Acad. Sci. USA* 97: 10905–10910.
24. Akiyama, T., Y. Shimo, H. Yanai, J. Qin, D. Ohshima, Y. Maruyama, Y. Asaumi, J. Kitazawa, H. Takayanagi, J. M. Penninger, et al. 2008. The tumor necrosis factor family receptors RANK and CD40 cooperatively establish the thymic medullary microenvironment and self-tolerance. *Immunity* 29: 423–437.
25. Hikosaka, Y., T. Nitta, I. Ohigashi, K. Yano, N. Ishimaru, Y. Hayashi, M. Matsumoto, K. Matsuo, J. M. Penninger, H. Takayanagi, et al. 2008. The cytokine RANKL produced by positively selected thymocytes fosters medullary thymic epithelial cells that express autoimmune regulator. *Immunity* 29: 438–450.
26. Wong, B. R., R. Josien, S. Y. Lee, B. Sauter, H. L. Li, R. M. Steinman, and Y. Choi. 1997. TRANCE (tumor necrosis factor [TNF]-related activation-induced cytokine), a new TNF family member predominantly expressed in T cells, is a dendritic cell-specific survival factor. *J. Exp. Med.* 186: 2075–2080.
27. Fata, J. E., Y. Y. Kong, J. Li, T. Sasaki, J. Irie-Sasaki, R. A. Moorehead, R. Elliott, S. Scully, E. B. Voura, D. L. Lacey, et al. 2000. The osteoclast differentiation factor osteoprotegerin-ligand is essential for mammary gland development. *Cell* 103: 41–50.
28. Yoshida, H., A. Naito, J. Inoue, M. Satoh, S. M. Santee-Cooper, C. F. Ware, A. Togawa, and S. Nishikawa. 2002. Different cytokines induce surface lymphotoxin-$\alpha\beta$ on IL-7 receptor-α cells that differentially engender lymph nodes and Peyer's patches. *Immunity* 17: 823–833.
29. Taylor, R. T., S. R. Patel, E. Lin, B. R. Butler, J. G. Lake, R. D. Newberry, and I. R. Williams. 2007. Lymphotoxin-independent expression of TNF-related activation-induced cytokine by stromal cells in cryptopatches, isolated lymphoid follicles, and Peyer's patches. *J. Immunol.* 178: 5659–5667.
30. Katakai, T., H. Suto, M. Sugai, H. Gonda, A. Togawa, S. Suematsu, Y. Ebisuno, K. Katagiri, T. Kinashi, and A. Shimizu. 2008. Organizer-like reticular stromal cell layer common to adult secondary lymphoid organs. *J. Immunol.* 181: 6189–6200.
31. Kim, D., R. E. Mebius, J. D. MacMicking, S. Jung, T. Cupedo, Y. Castellanos, J. Rho, B. R. Wong, R. Josien, N. Kim, et al. 2000. Regulation of peripheral lymph node genesis by the tumor necrosis factor family member TRANCE. *J. Exp. Med.* 192: 1467–1478.
32. Kubota, K., C. Sakikawa, M. Katsumata, T. Nakamura, and K. Wakabayashi. 2002. Platelet-derived growth factor BB secreted from osteoclasts acts as an osteoblastogenesis inhibitory factor. *J. Bone Miner. Res.* 17: 257–265.
33. Pappo, J., and T. H. Ermak. 1989. Uptake and translocation of fluorescent latex particles by rabbit Peyer's patch follicle epithelium: a quantitative model for M cell uptake. *Clin. Exp. Immunol.* 76: 144–148.
34. Chabot, S., J. S. Wagner, S. Farrant, and M. R. Neutra. 2006. TLRs regulate the gatekeeping functions of the intestinal follicle-associated epithelium. *J. Immunol.* 176: 4275–4283.
35. Terahara, K., M. Yoshida, O. Igarashi, T. Nochi, G. S. Pontes, K. Hase, H. Ohno, S. Kurokawa, M. Mejima, N. Takayama, et al. 2008. Comprehensive gene expression profiling of Peyer's patch M cells, villous M-like cells, and intestinal epithelial cells. *J. Immunol.* 180: 7840–7846.
36. Kamijo, S., A. Nakajima, K. Ikeda, K. Aoki, K. Ohya, H. Akiba, H. Yagita, and K. Okumura. 2006. Amelioration of bone loss in collagen-induced arthritis by neutralizing anti-RANKL monoclonal antibody. *Biochem. Biophys. Res. Commun.* 347: 124–132.
37. Golovkina, T. V., M. Shlomchik, L. Hannum, and A. Chervonsky. 1999. Organogenic role of B lymphocytes in mucosal immunity. *Science* 286: 1965–1968.
38. Lugering, A., M. Floer, S. Westphal, C. Maaser, T. W. Spahn, M. A. Schmidt, W. Domschke, I. R. Williams, and T. Kucharzik. 2005. Absence of CCR6 inhibits $CD4^+$ regulatory T-cell development and M-cell formation inside Peyer's patches. *Am. J. Pathol.* 166: 1647–1654.
39. Neutra, M. R., N. J. Mantis, and J. P. Kraehenbuhl. 2001. Collaboration of epithelial cells with organized mucosal lymphoid tissues. *Nat. Immunol.* 2: 1004–1009.
40. Kunisawa, J., T. Nochi, and H. Kiyono. 2008. Immunological commonalities and distinctions between airway and digestive immunity. *Trends Immunol.* 29: 505–513.
41. des Rieux, A., V. Fievez, I. Theate, J. Mast, V. Preat, and Y. J. Schneider. 2007. An improved in vitro model of human intestinal follicle-associated epithelium to study nanoparticle transport by M cells. *Eur. J. Pharm. Sci.* 30: 380–391.
42. Williamson, E., J. M. Bilsborough, and J. L. Viney. 2002. Regulation of mucosal dendritic cell function by receptor activator of NF-κB (RANK)/RANK ligand interactions: impact on tolerance induction. *J. Immunol.* 169: 3606–3612.
43. Totsuka, T., T. Kanai, Y. Nemoto, T. Tomita, R. Okamoto, K. Tsuchiya, T. Nakamura, N. Sakamoto, H. Akiba, K. Okumura, et al. 2009. RANK-RANKL signaling pathway is critically involved in the function of $CD4^+CD25^+$ regulatory T cells in chronic colitis. *J. Immunol.* 182: 6079–6087.
44. Pfeffer, K. 2003. Biological functions of tumor necrosis factor cytokines and their receptors. *Cytokine Growth Factor Rev.* 14: 185–191.
45. Foxwell, A. R., A. W. Cripps, and J. M. Kyd. 2007. Optimization of oral immunization through receptor-mediated targeting of M cells. *Hum. Vaccin.* 3: 220–223.
46. Chionh, Y. T., J. L. Wee, A. L. Every, G. Z. Ng, and P. Sutton. 2009. M-cell targeting of whole killed bacteria induces protective immunity against gastrointestinal pathogens. *Infect. Immun.* 77: 2962–2970.
47. Nochi, T., Y. Yuki, A. Matsumura, M. Mejima, K. Terahara, D. Y. Kim, S. Fukuyama, K. Iwatsuki-Horimoto, Y. Kawaoka, T. Kohda, et al. 2007. A novel M cell-specific carbohydrate-targeted mucosal vaccine effectively induces antigen-specific immune responses. *J. Exp. Med.* 204: 2789–2796.

Published October 26, 2009

JEM

ARTICLE

Id2-, RORγt-, and LTβR-independent initiation of lymphoid organogenesis in ocular immunity

Takahiro Nagatake,[1,5] Satoshi Fukuyama,[1] Dong-Young Kim,[1,6] Kaoru Goda,[1] Osamu Igarashi,[1] Shintaro Sato,[1] Tomonori Nochi,[1] Hiroshi Sagara,[2] Yoshifumi Yokota,[7] Anton M. Jetten,[8] Tsuneyasu Kaisho,[9] Shizuo Akira,[10] Hitomi Mimuro,[3] Chihiro Sasakawa,[3] Yoshinori Fukui,[11] Kohtaro Fujihashi,[12] Taishin Akiyama,[4] Jun-ichiro Inoue,[4] Josef M. Penninger,[13] Jun Kunisawa,[1,14] and Hiroshi Kiyono[1,5,12,14]

[1]Division of Mucosal Immunology, Department of Microbiology and Immunology, [2]Medical Proteomics Laboratory, [3]Division of Bacterial Infection, Department of Microbiology and Immunology, and [4]Division of Cellular and Molecular Biology, The Institute of Medical Science, The University of Tokyo, Minato-ku, Tokyo 108-8639, Japan
[5]Graduate School of Medicine and Faculty of Medicine, The University of Tokyo, Bunkyo-ku, Tokyo 113-0033, Japan
[6]Department of Otorhinolaryngology, Seoul National University College of Medicine, Chongno-gu, Seoul 110-744, Korea
[7]Department of Molecular Genetics, School of Medicine, University of Fukui, Eiheiji-cho, Yoshida-gun, Fukui 910-1193, Japan
[8]Cell Biology Section, Laboratory of Respiratory Biology, National Institute of Environmental Health Sciences, National Institutes of Health, Research Triangle Park, NC 27709
[9]Laboratory for Host Defense, Research Center for Allergy and Immunology, Institute of Physical and Chemical Research, Tsurumi-ku, Yokohama, Kanagawa 230-0045, Japan
[10]Laboratory of Host Defense, World Premier International Research Center-Immunology Frontier Research Center, Osaka University, Suita, Osaka 565-0871, Japan
[11]Division of Immunogenetics, Department of Immunobiology and Neuroscience, Medical Institute of Bioregulation, Kyushu University, Fukuoka 812-8582, Japan
[12]Immunobiology Vaccine Center, Department of Pediatric Dentistry, The University of Alabama at Birmingham, Birmingham, AL 35294
[13]Institute of Molecular Biotechnology of the Austrian Academy of Sciences, 1030 Vienna, Austria
[14]Graduate School of Frontier Sciences, The University of Tokyo, Kashiwa, Chiba 277-8561, Japan

CORRESPONDENCE
Hiroshi Kiyono:
kiyono@ims.u-tokyo.ac.jp

The eye is protected by the ocular immunosurveillance system. We show that tear duct–associated lymphoid tissue (TALT) is located in the mouse lacrimal sac and shares immunological characteristics with mucosa-associated lymphoid tissues (MALTs), including the presence of M cells and immunocompetent cells for antigen uptake and subsequent generation of mucosal immune responses against ocularly encountered antigens and bacteria such as *Pseudomonas aeruginosa*. Initiation of TALT genesis began postnatally; it occurred even in germ-free conditions and was independent of signaling through organogenesis regulators, including inhibitor of DNA binding/differentiation 2, retinoic acid–related orphan receptor γt, lymphotoxin (LT) α1β2–LTβR, and lymphoid chemokines (CCL19, CCL21, and CXCL13). Thus, TALT shares immunological features with MALT but has a distinct tissue genesis mechanism and plays a key role in ocular immunity.

Abbreviations used: AID, activation-induced cytidine deaminase; CALT, conjunctiva-associated lymphoid tissue; CT, cholera toxin; FAE, follicle-associated epithelium; FDC, follicular DC; GC, germinal center; HE, hematoxylin and eosin; HEV, high endothelial venule; Id2, inhibitor of DNA binding/differentiation 2; ILF, isolated lymphoid follicle; LT, lymphotoxin; LTi, lymphoid tissue inducer; MAdCAM-1, mucosal addressin cell adhesion molecule 1; MALT, mucosa-associated lymphoid tissue; NALT, nasopharynx-associated lymphoid tissue; NIK, NF-κB–inducing kinase; NP, nasal passage; pLN, peripheral LN; PNA, peanut agglutinin; PNAd, pLN addressin; PP, Peyer's patch; ROR, retinoic acid–related orphan receptor; TALT, tear duct–associated lymphoid tissue; TLR, Toll-like receptor; TRAF, TNF receptor–associated factor; TRANCE, TNF-related activation-induced cytokine; UEA, *Ulex europaeus* agglutinin; VCAM-1, vascular cell adhesion molecule 1.

Mucosa-associated lymphoid tissues (MALTs), including nasopharynx-associated lymphoid tissue (NALT) and Peyer's patches (PPs), are gateways for the uptake of inhaled and ingested antigens from the lumen of the aerodigestive tract, and are considered to be the sites of induction of mucosal immune responses (Mestecky et al., 2003; Kiyono and Fukuyama, 2004). The ocular surface leading to the lacrimal sac and nasolacrimal duct also forms an interface with the outside environment. In fact, it has been proposed that conjunctiva-associated lymphoid tissue (CALT), together with tear duct–associated lymphoid tissue (TALT), organizes eye-associated lymphoid tissue to create mucosal surveillance and a barrier in the eye

The Rockefeller University Press $30.00
J. Exp. Med. Vol. 206 No. 11 2351-2364
www.jem.org/cgi/doi/10.1084/jem.20091436

Supplemental Material can be found at:
http://jem.rupress.org/content/suppl/2009/10/12/jem.20091436.DC1.html

Published October 26, 2009

region of humans (Knop and Knop, 2000, 2001). Past investigations have focused on the identification and characterization of CALT (Gomes et al., 1997; Chodosh et al., 1998; Knop and Knop, 2000, 2005; Giuliano et al., 2002; Cain and Phillips, 2008). Mice and rats do not possess CALT, whereas other mammals (e.g., cats, dogs, and humans) do develop CALT (Chodosh et al., 1998). Rat conjunctivae, lacrimal glands, and harderian glands contain immunocompetent cells (e.g., $CD4^+$ and $CD8^+$ cells; Gomes et al., 1997); however, the immunocompetent cells do not form any organized microarchitecture at the conjunctiva and are thus diffusely located. Tears contain cytokines (e.g., IL-1, IL-4, IL-6, and TGF-β), antimicrobial peptides (e.g., lactoferrin and defensin), and secretory IgA; these secretions are an important arm of mucosal innate and acquired immunity, and respond to antigens that contact and invade the eye (Allansmith et al., 1985; Kijlstra, 1990; Gupta et al., 1996; Haynes et al., 1998; Nakamura et al., 1998; Uchio et al., 2000). Tear flow does not just provide mucosal protection at the ocular surface; it also connects the ocular surface with the nasal cavity via the tear duct, suggesting that tear flow is integral to regulating the homeostasis of the oculonasal mucosal barrier. On the other hand, the eye is considered to be an immune-privileged site, because the microenvironment of the eye is regulated by several complex aspects of the immune system (Stein-Streilein and Taylor, 2007). However, little information is currently available about the immunological nature of the eye-associated lymphoid tissue system—particularly the regulation of the tissue genesis of TALT and its immunological functions—despite the fact that TALT develops in humans (Knop and Knop, 2000, 2001).

Organogenesis of secondary lymphoid tissues, such as PPs and peripheral LNs (pLNs), is dependent on inflammatory cytokines, the release of which is mediated by lymphotoxin (LT) β receptor (LTβR) signals during the embryonic period (Mebius, 2003). The basis of LT-mediated lymphoid organ development at a molecular level was first shown in genetically manipulated $Lt\alpha^{-/-}$ mice, which lack PPs and pLNs (De Togni et al., 1994). Injection of an agonistic LTβR antibody into $Lt\alpha^{-/-}$ mice during a limited period in embryogenesis regenerates pLNs (Rennert et al., 1998). The physiological ligand of LTβR is a membrane-bound form of $LT\alpha1\beta2$ produced by $CD3^-CD4^+CD45^+$ lymphoid tissue inducer (LTi) cells expressing IL-7Rα (Mebius et al., 1997). IL-7Rα–mediated signals trigger LTi cells to produce $LT\alpha1\beta2$, and $Il\text{-}7r\alpha^{-/-}$ mice do not form PPs (Adachi et al., 1998b; Honda et al., 2001). In addition, deficiency of either inhibitor of DNA binding/differentiation 2 (Id2) or the retinoic acid–related orphan receptor (ROR) γt gene results in a lack of PPs and pLNs because the differentiation of $CD3^-CD4^+CD45^+$ LTi cells is impaired (Yokota et al., 1999; Sun et al., 2000; Eberl et al., 2004). These facts indicate the importance of inflammation-related cytokines, as well as Id2- and RORγt-subordinated $CD3^-CD4^+CD45^+$ LTi cells, in the organogenesis of lymphoid tissues, including PPs and pLNs (Kiyono and Fukuyama, 2004). However, NALT does not follow the general biological rule of the dependence of embryonic genesis on inflammatory cytokines (Fukuyama et al., 2002; Harmsen et al., 2002). NALT organogenesis, which occurs postnatally, is independent of LTβR-mediated signals and RORγt but does require Id2 (Fukuyama et al., 2002; Harmsen et al., 2002).

In this study, we provide evidence that TALT develops independently of organogenesis regulators, a finding that distinguishes TALT genesis from that of other lymphoid organs. In addition, we found that TALT plays a central role in the induction of antigen-specific immune responses against ocularly encountered antigens.

RESULTS

Identification of TALT in mice

TALT develops in the human tear duct (Knop and Knop, 2000, 2001; Paulsen et al., 2000, 2003), but to our knowledge no information is currently available on TALT in mice. To identify organized lymphoid tissue in the mouse tear duct and to elucidate its immunological and developmental features, we first examined the anatomy of this duct in mice. To visualize the position of the tear duct, we administered hematoxylin to mice in eye drops. We clearly observed the location of the tear duct where it connects the ocular surface to the nasal cavity (Fig. 1 A). In coronal and horizontal views, we were able to identify TALT in both the left and right side of the lacrimal sac in C57BL/6 WT mice (Fig. 1, B and C).

Postnatal development of TALT

The genesis of each type of lymphoid tissue occurs within a given time window: for example, PPs develop during late embryogenesis and NALT develops postnatally (Fukuyama et al., 2002; Mebius, 2003; Kiyono and Fukuyama, 2004). The initiation of intestinal isolated lymphoid follicles (ILFs) also occurs after birth, and the genetic background (e.g., whether the mouse is of the C57BL/6 or BALB/c strain) influences the postnatal time of initiation of tissue genesis (Hamada et al., 2002). To determine when TALT genesis is initiated and to evaluate the influence of genetic background on tissue genesis, we took tissue samples from both C57BL/6 and BALB/c mice at various pre- and postnatal stages for histological analysis. No sign of mononuclear cell accumulation was observed at embryonic day (E) 18 or postnatal day (D) 5 in C57BL/6 or BALB/c mice (Fig. 1 D and Fig. S1). In contrast, we detected accumulation of mononuclear cells at D10 in both C57BL/6 and BALB/c mice, indicating that the TALT development was initiated between D5 and D10, and that the different genetics of the two strains did not influence TALT organogenesis (Fig. 1 D and Fig. S1). To support the data, the initial appearance of mononuclear cells was noted at D7 in both C57BL/6 and BALB/c mice (Fig. 1 D and Fig. S1). Furthermore, pLN addressin (PNAd)–positive high endothelial venules (HEVs) developed at D10 but not at D5 and D7 (Fig. 1 E). These findings suggest that TALT develops postnatally, as does NALT. Unlike in the genesis

Published October 26, 2009

of other lymphoid tissues (Mebius, 2003), expression of vascular cell adhesion molecule 1 (VCAM-1) was not observed at the TALT anlage (unpublished data).

To determine which cell population initially migrates to the TALT anlage, we analyzed the tissue genesis site at D5, D7, and D10 by confocal microscopy. The D5 anlagen did not

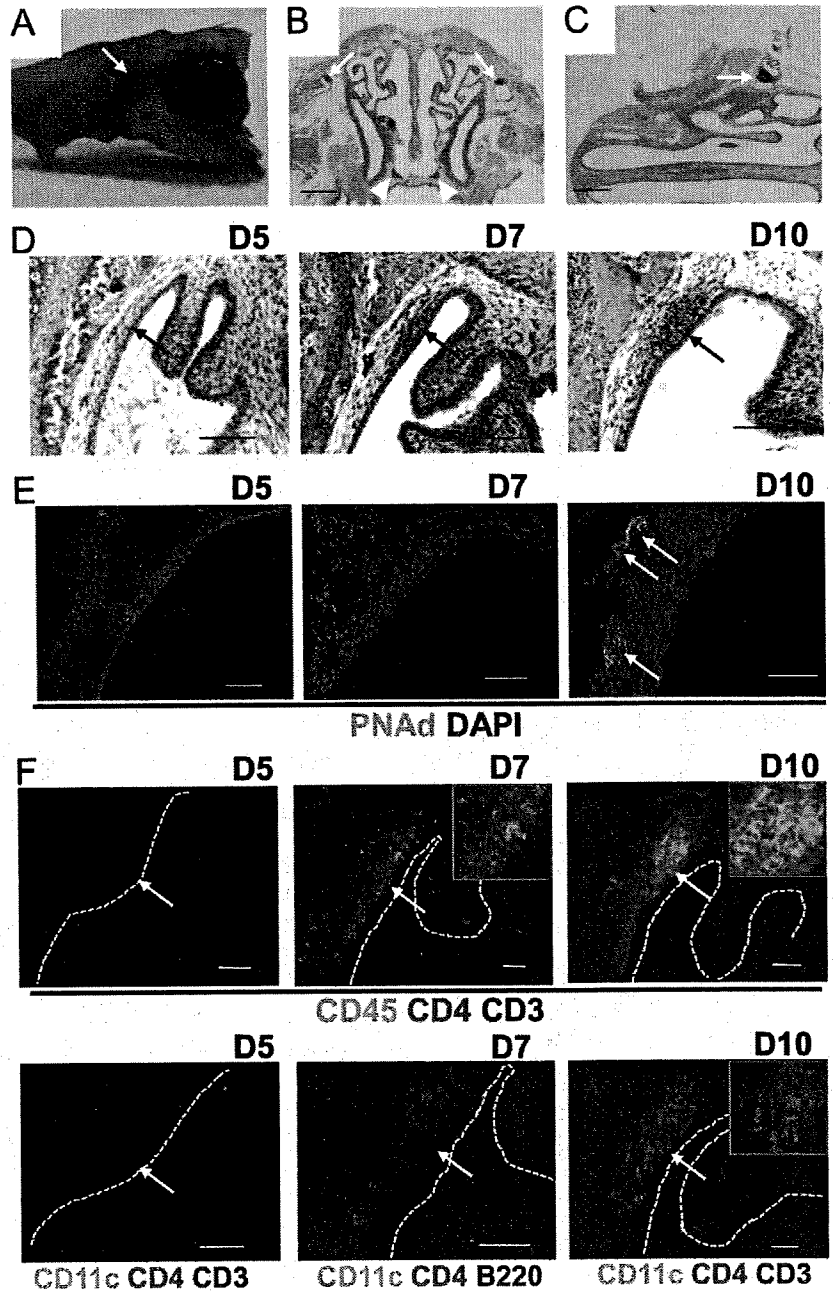

Figure 1. Postnatal development of TALT. (A–C) 10 µl of hematoxylin solution was added to the ocular surface of 8-wk-old C57BL/6 mice to visualize the tear duct (A, arrow). Coronal (B) and horizontal (C) paraffinized sections of the head were stained with HE. Arrows and arrowheads indicate TALT and NALT, respectively (n = 3 mice/group). Bars, 1 mm. (D) Paraffinized tissues of heads from D5, D7, and D10 C57BL/6 mice were examined by HE staining. Arrows indicate the site of TALT genesis (n = 5 mice/group). Bars, 100 µm. (E and F) Head tissue of C57BL/6 mice was examined by confocal microscopy with the indicated antibodies at D5, D7, and D10. Arrows indicate PNAd$^+$ HEVs (E) and the site of TALT genesis (F). Some magnified pictures are shown in F (insets). Dashed lines indicate the edge between the TALT epithelium and tear duct lumen. These data are representative of at least three independent experiments (n = 5 mice/group). Bars, 50 µm.

Published October 26, 2009

JEM

contain any CD45$^+$ cells, whereas the D7 TALT anlage possessed CD45$^+$ cells (Fig. 1 F). CD3$^-$CD4$^+$CD45$^+$ cells have been shown to be LTi cells (Mebius, 2003). Among the CD45$^+$ cells in the D7 TALT anlage, we identified CD3$^-$CD4$^+$CD45$^+$ cells and B220$^+$ B cells (Fig. 1 F, D7). CD11c$^+$ DCs were not found at D5 and D7. At D10, CD11c$^+$ DCs and increased numbers of CD3$^-$CD4$^+$CD45$^+$ cells were found in the TALT (Fig. 1 F). Because B220$^+$ B cells were among the first cells to migrate at the TALT anlage (Fig. 1 F, D7), we examined B cell–deficient *Igh6*$^{-/-}$ mice for the development of TALT. The TALT genesis occurred normally, even in the B cell–deficient condition (Fig. S2 A). Further, TALT also developed in T cell–deficient *Tcrβ*$^{-/-}$, *Tcrδ*$^{-/-}$ mice (Fig. S2 B). These findings show that B and T lymphocytes and DCs are dispensable for the initiation of TALT development.

Organogenesis of TALT does not require microbial stimulation

TALT has been identified in only 30–40% of humans examined (Paulsen et al., 2000, 2003; Knop and Knop, 2001), raising the possibility that environmental conditions, including microbial infections and allergic responses, are involved in the initiation of TALT development. In addition, our finding that TALT develops postnatally also points to the possible involvement of microbial stimulation in TALT genesis. However, we detected TALT in mice deficient in Toll-like receptor (TLR) signals, including *Tlr2*$^{-/-}$, *Tlr4*$^{-/-}$, and *MyD88*$^{-/-}$ mice (Fig. S2, C–E). Further, we found that germ-free mice developed TALT (Fig. 2 A). Thus, TALT organogenesis is most likely independent of microbial stimulation.

TALT development is independent of organogenesis regulators

We next determined the molecular requirements for TALT development. PPs and pLNs are not present in alymphoplasia (*aly/aly*) mice, which carry a null mutation of NF-κB–inducing kinase (NIK), resulting in a failure to transmit LTβR-mediated signals (Shinkura et al., 1999). However, our histological analysis showed that the TALT structure was preserved in *aly/aly* and *Ltα*$^{-/-}$ mice, although it was smaller than in WT TALT (Fig. 2, A and B; and Fig. S3). In addition, TALT was even observed in *Il-7rα*$^{-/-}$ mice, although the size was again small (Fig. 2 B and Fig. S3). Thus, the initiation of TALT development mediated by inducer cells was independent of the IL-7R and LTα1β2–LTβR–NIK pathway signaling cascades, whereas the maturation process of accumulating lymphocytes required the cytokine signaling cascade, as is the case with other lymphoid organs (Mebius, 2003; Kiyono and Fukuyama, 2004).

Lymphoid chemokines, including CXCL13, CCL19, and CCL21, play important roles in the migration of LTi cells to the sites of tissue genesis (Honda et al., 2001; Luther et al., 2003; Fukuyama et al., 2006). We therefore examined the involvement of these lymphoid chemokines in TALT genesis. The TALT structure was preserved in *Cxcl13*$^{-/-}$ mice, although they lacked some pLNs and had reduced numbers of PPs (Fig. 2 B; Ansel et al., 2000). TALT also developed well in *plt/plt* mice (Fig. 2 B), which carry null mutations of both the *Ccl19* and *Ccl21* genes (Nakano et al., 1998). Furthermore, the initiation of TALT formation was maintained in triple mutant (*Cxcl13*$^{-/-}$ *plt/plt*) mice (Fig. 2 B), confirming that these lymphoid chemokines are not required for the initiation of TALT organogenesis, although the TALT was smaller in the lymphoid chemokine–null condition than in WT (Fig. S3). These results supported the observation that an NIK-mediated pathway is required to recruit large numbers of lymphocytes to TALT.

We then addressed the involvement of Id2 and RORγt, key transcriptional regulators in the induction of lymphoid organogenesis by CD3$^-$CD4$^+$CD45$^+$ LTi cells (Yokota et al., 1999; Sun et al., 2000; Eberl et al., 2004). Surprisingly, TALT formation was preserved in *Id2*$^{-/-}$ and *Rorγt*$^{-/-}$ mice (Fig. 2 B). Consistent with this finding, FACS and confocal microscopy analyses detected CD3$^-$CD4$^+$ LTi cells in the TALT anlage of *Id2*$^{-/-}$ and *Rorγt*$^{-/-}$ mice as well as in WT mice (Fig. 3, A and B). Furthermore, when we isolated these CD3$^-$CD4$^+$CD45$^+$ cells from WT mice and examined the gene expression of the tissue genesis–associated transcription factors by RT-PCR, we found that CD3$^-$CD4$^+$CD45$^+$ cells isolated from the TALT anlagen did not express either *Id2* or *Rorγt*, whereas CD3$^-$CD4$^+$CD45$^+$ cells isolated from the embryonic intestine, i.e., PP inducer cells, expressed both *Id2* and *Rorγt* (Fig. 3 C). Thus, TALT organogenesis proceeds independently of Id2, RORγt, and LT. Therefore, TALT genesis is quite different from the genesis of other secondary lymphoid tissues, including PPs, pLNs, and NALT (Mebius, 2003; Kiyono and Fukuyama, 2004).

Microarchitecture of TALT

The structure of the MALT epithelium is characterized by the presence of follicle-associated epithelium (FAE; Kiyono and Fukuyama, 2004). Indeed, we were able to divide the epithelial layer of the lacrimal sac into two populations on the basis of its morphological structure (Fig. 4 A): TALT-FAE was characterized by a thin layer of squamous epithelium (Fig. 4 B), whereas the lacrimal sac epithelium had a multilayered and squamous morphology (Fig. 4 C). Interestingly, TALT-FAE lacked mucus-producing goblet cells and cilia (Fig. 4 B), a fact that distinguished this tissue from NALT-FAE, which has some goblet cells (Fig. 4 D). Instead, mucus-producing gland tissue was frequently observed on the conjunctiva (unpublished data). Confocal microscopic analysis of TALT revealed large numbers of B220$^+$ B cells (Fig. 4 E) and CD11c$^+$ DCs in the subepithelial dome region of the FAE (Fig. 4 F), as well as CD3$^+$CD4$^+$ T helper cells distributed around the B cell follicles (Fig. 4, G and H). These data indicate that TALT is composed of a highly compartmentalized and organized lymphoid structure. In accordance with the finding that neonatal TALT developed PNAd$^+$ HEVs (Fig. 1 E), adult TALT HEVs expressed PNAd but not mucosal addressin cell adhesion molecule 1 (MAdCAM-1; Fig. 4 I and Fig. S4 A); this is similar to the case with NALT HEVs

Published October 26, 2009

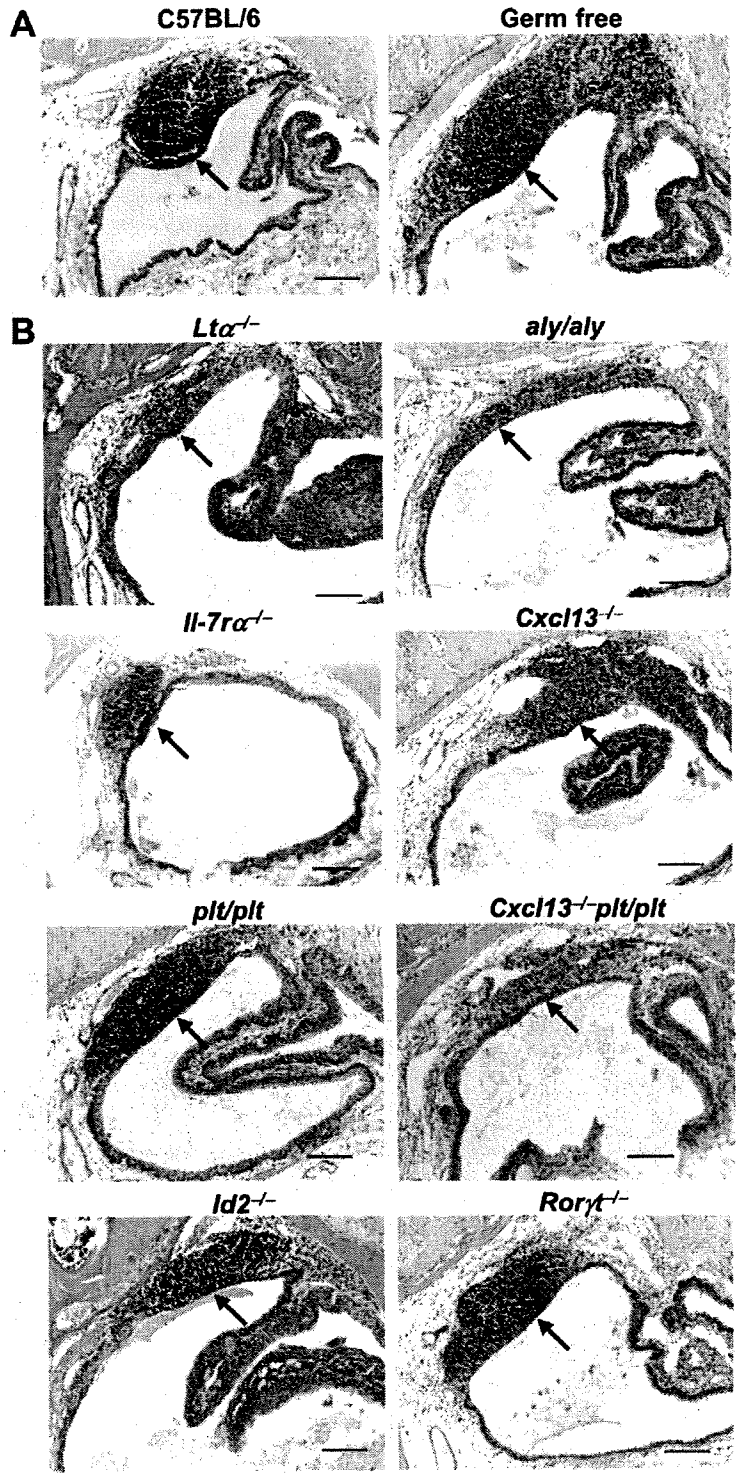

Figure 2. TALT genesis is independent of microbial stimulation and organogenesis-associated molecules. Paraffin-embedded tissue sections were analyzed by HE staining for TALT development. (A) The presence of TALT in germ-free mice, as well as C57BL/6 WT mice, shows that TALT develops independently of microbial stimulation (n = 3 mice/group). (B) Development of TALT in 8-wk-old *Lt$\alpha^{-/-}$*, *aly/aly*, *Il-7r$\alpha^{-/-}$*, *Cxcl13$^{-/-}$*, *plt/plt*, *Cxcl13$^{-/-}$plt/plt*, *Id2$^{-/-}$*, and *Rorγt$^{-/-}$* mice shows that the initiation of TALT development occurs independently of organogenesis-associated molecules. Arrows indicate the presence of TALT. These data are representative of at least three independent experiments per group (n = 5 mice/group). Bars, 100 µm.

Published October 26, 2009

(Fig. 4 J and Fig. S4 B). These observations suggest that cellular trafficking to TALT and NALT is regulated via an L-selectin–PNAd interaction and is distinguishable from gut-trafficking mechanisms, which are dependent on α4β7 integrin/MAdCAM-1 (Kiyono and Fukuyama, 2004). These results indicate that TALT possesses many of the characteristic traits of organized MALT but is distinguished by the lack of goblet cells in its FAE region.

TALT is a site of immunological induction

To investigate the physiological function of TALT, we examined whether TALT takes up ocularly administered antigens. M cells, characterized by the M cell–specific mAb NKM16-2-4$^+$ (Nochi et al., 2007), *Ulex europaeus* agglutinin (UEA) 1$^+$, and wheat germ agglutinin$^-$, were found in the FAE of TALT (Fig. 5 A). Electron microscopic analysis showed that TALT-FAE contained cells bearing the hallmarks of M cells: microvilli and a unique pocket formation with lymphocytes (Fig. 5, B and C). When mice were ocularly dosed with GFP-expressing *Salmonella*, we observed the uptake of *Salmonella* by UEA-1$^+$ M cells (Fig. 5 D) as well as by CD11c$^+$ DCs (Fig. 5 E). Moreover, when mice were ocularly challenged with *Pseudomonas aeruginosa* PAO1, large amounts of *P. aeruginosa* PAO1 were located within the TALT (Fig. 5 F). *P. aeruginosa* PAO1 was not detected in naive mice (Fig. 5 G). Mice ocularly challenged with *P. aeruginosa* PAO1 formed germinal centers (GCs; Fig. 5 H); this is an important immunological event for the initiation of hypersomatic mutations and Ig class switching, which enable the production of memory B cells with high-affinity B cell receptors (Kelsoe, 1996; Shapiro-Shelef and Calame, 2005). In contrast, GC formation was not present in the TALT of naive mice (Fig. 5 I; and Fig. 6, A and B). These data suggest that TALT is a preferential site for the uptake of ocularly encountered antigens/pathogens and for the subsequent induction of antigen-specific B cell responses.

Supporting this notion, immunization of the eyes with eye drops containing cholera toxin (CT), a well-known mucosal immunogen, resulted in the formation of GCs with a follicular DC (FDC) network in the TALT (Fig. 6, C and D). Interestingly, ocular immunization also induced GC formation in NALT (Fig. 6, E and F), suggesting that the anatomical

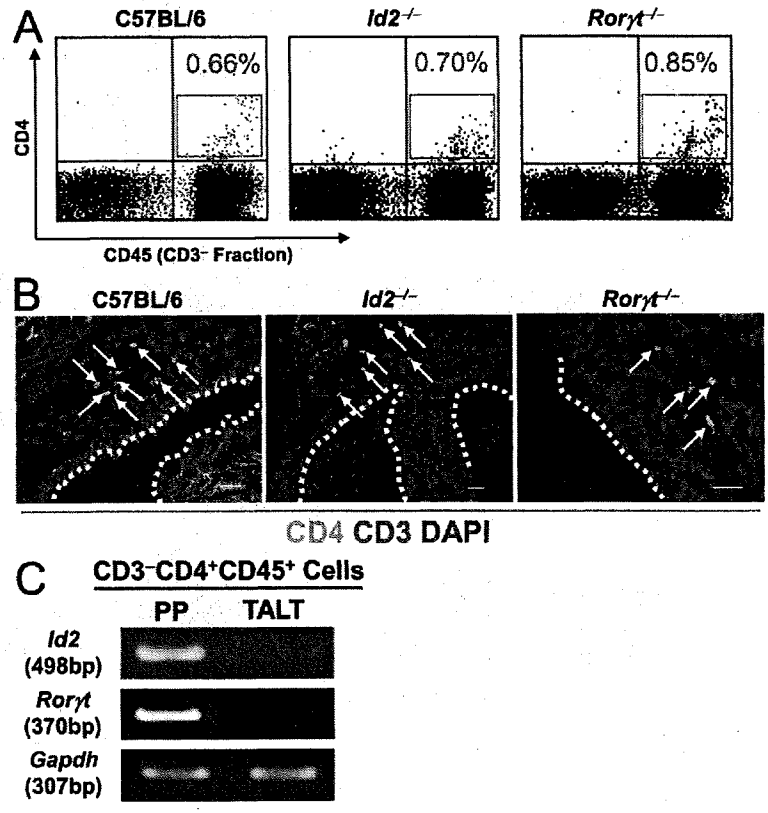

Figure 3. Presence of CD3$^-$CD4$^+$CD45$^+$ cells in the TALT anlagen. (A) Because substantial numbers of CD3$^-$CD4$^+$CD45$^+$ cells were noted in the TALT anlagen of D10 mice, we analyzed mononuclear cells from D10 tear ducts by FACS. Percentages of CD3$^-$CD4$^+$CD45$^+$ cells are shown in red (n = 6 mice/group). (B) Confocal microscopic analysis of the site of TALT genesis at D10. Frozen tissue samples were stained with the antibodies indicated. Arrows point to CD3$^-$CD4$^+$ cells (n = 6 mice/group). Dotted lines indicate the edge between the TALT epithelium and tear duct lumen. Bars, 50 µm. (C) CD3$^-$CD4$^+$CD45$^+$ cells from PP and TALT were isolated from an E17 intestine and D10 tear duct, respectively. Gene expression of *Id2* and *Rorγt* were analyzed by RT-PCR. The expression of *Gapdh* is shown as an internal control. These data are representative of at least three independent experiments (n = 18–20 mice/group).

Published October 26, 2009

connection through the tear duct lays the groundwork for a cooperative immunological network between TALT and NALT that responds to ocularly encountered antigens. Activation-induced cytidine deaminase (AID), an essential Ig class switch–related molecule, is expressed in organized lymphoid tissues, including NALT, PPs, and intestinal ILFs (Shikina et al., 2004). Parallel to our findings of GC formation after ocular immunization, confocal microscopy revealed the presence

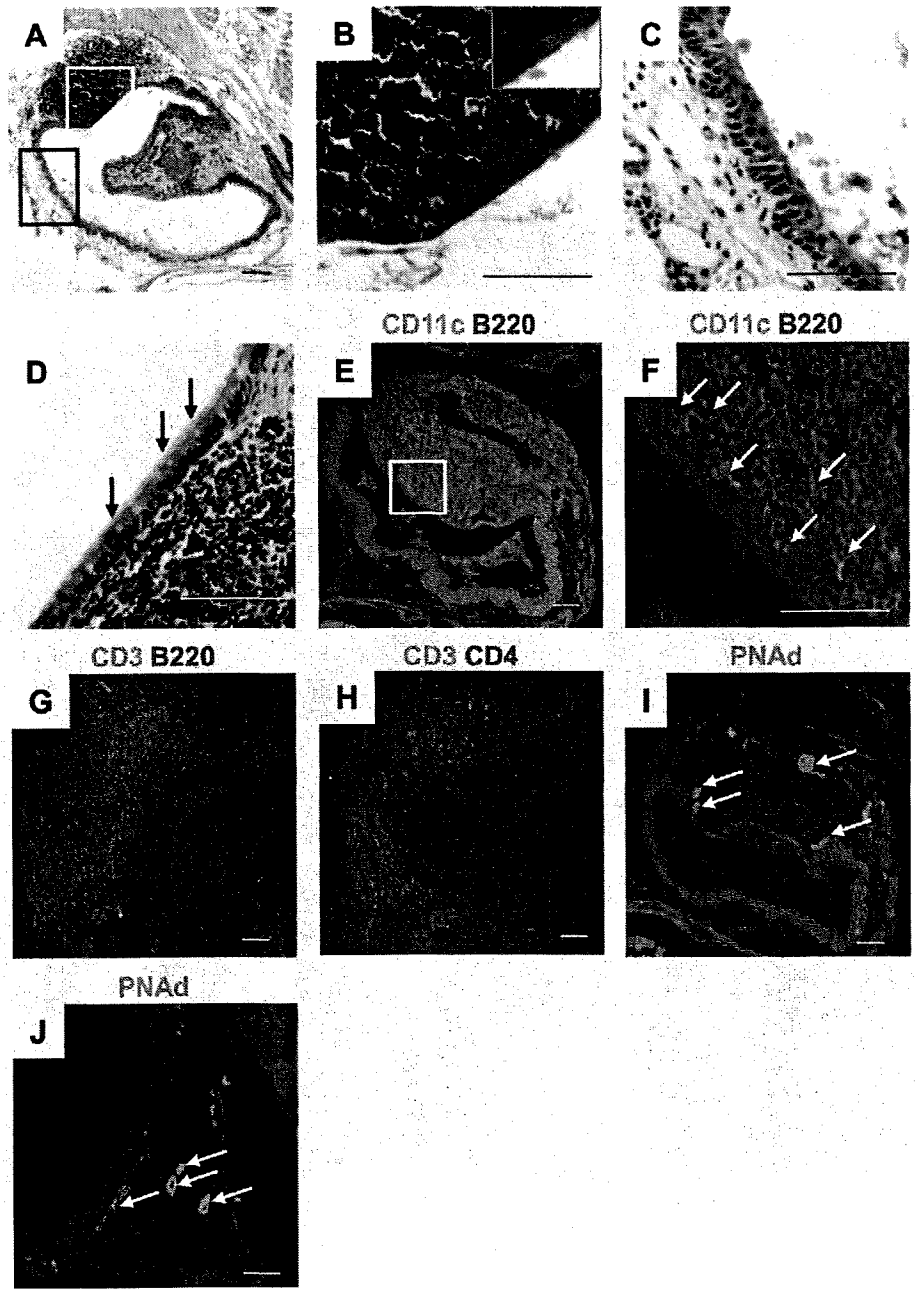

Figure 4. Microarchitecture of TALT. (A–C) The epithelial region of TALT in WT mice was analyzed by HE staining. B and C are magnifications, respectively, of the white and black boxes in A, and show TALT-FAE (B) and the lacrimal sac epithelium (C). The inset in B shows single-layered squamous epithelium in the TALT FAE (n = 3 mice/group). (D) The presence of goblet cells in NALT-FAE is indicated by arrows (n = 3 mice). (E–J) Confocal microscopic analysis of TALT (E–I) and NALT (J) in C57BL/6 WT mice. Tissue samples were stained with the antibodies indicated. F is a magnified view of the box in E; arrows point to the presence of CD11c$^+$ DCs. Arrows in I and J indicate PNAd$^+$ HEVs. These data are representative of at least three independent experiments (n = 3 mice/group). Bars, 50 µm.

Published October 26, 2009

of AID-expressing cells in both TALT and NALT (Fig. 6, G, and H). Furthermore, RT-PCR analysis confirmed *Aid* expression in TALT and NALT but not in the nasal passage (NP; Fig. 6 I). Therefore, after ocular immunization with CT, increased numbers of IgA^+B220^- plasma cells were detected in the diffuse region of the tear duct (Fig. 6, J and K). An ELISPOT assay confirmed that some of these IgA^+B220^- plasma cells produced CT-specific IgA; cells producing IgA specific for the B subunit of CT (CT-B), but not IgG-forming cells, were found in single-cell preparations from the tear ducts of mice ocularly immunized with CT (Fig. 6 L and not depicted). In addition, the production of CT-B–specific IgG-forming cells was induced in the spleen by ocular immunization with CT (Fig. 6 M). Naive mice did not show any CT-B–specific Ig-producing cells (Fig. 6 N).

In addition, we found a high frequency of CT-B–specific $CD4^+$ T cells in TALT using an MHC tetramer, consistent with the induction of antigen-specific antibody-producing

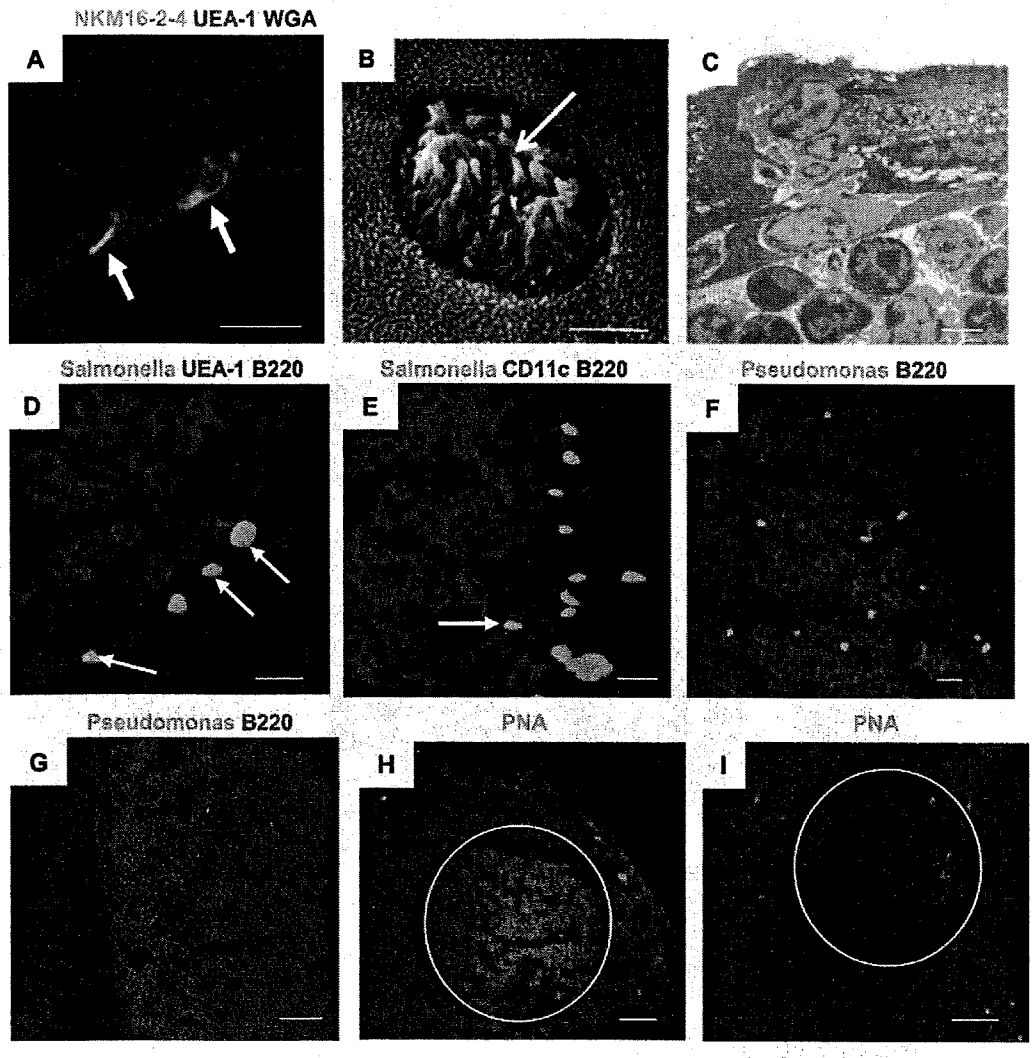

Figure 5. TALT is the site of ocular antigen uptake. (A) A confocal micrograph of TALT shows the presence of NKM16-2-4$^+$ UEA-1$^+$ M cells (arrows; $n = 3$ mice). Bar, 20 µm. (B and C) TALT-FAE was analyzed by scanning electron microscopy (B) and transmission electron microscopy (C). White and red arrows indicate M cells with the unique characteristics of microvilli and pocket lymphocytes, respectively ($n = 5$ mice/group). Bars, 3 µm. (D and E) Mice were given GFP-expressing *Salmonella* by eye drops. After 30 min, TALT was isolated and examined with confocal microscopy. Arrows in D and E point, respectively, to *Salmonella* captured by UEA-1$^+$ M cells and CD11c$^+$ DCs in TALT ($n = 3$ mice/group). Bars, 10 µm. (F) Mice were given *P. aeruginosa* PAO-1 by eye drops. After 30 min, TALT was isolated and examined with confocal microscopy. A large number of *P. aeruginosa* PAO-1 were found inside the TALT ($n = 3$ mice). Bar, 10 µm. (G) As a negative control for F, TALT from mice given PBS by eye drops were analyzed ($n = 3$ mice). Bar, 50 µm. (H) Mice were given *P. aeruginosa* PAO-1 by eye drops twice at an interval of 1 wk. 1 wk after the second administration, TALT was isolated and examined with confocal microscopy. GC formation was induced by ocular administration of *P. aeruginosa* PAO-1 ($n = 3$ mice). Bar, 50 µm. (I) TALT from a control naive mouse is shown. GCs did not form in naive TALT. These data are representative of at least two independent experiments per group ($n = 3$ mice). Bar, 50 µm.

Published October 26, 2009

cells after CT immunization (Fig. 7 A). It is important to note that the CT-B tetramer–reactive $CD4^+$ T cells included $CXCR5^+$ T follicular helper cells (Fig. 7 B). CT-B–specific $CD4^+$ T cells were detected in NALT and draining LNs, such as the cervical and submandibular LNs, but at a lower frequency than in TALT (Fig. 7, A and B). Thus, it is plausible

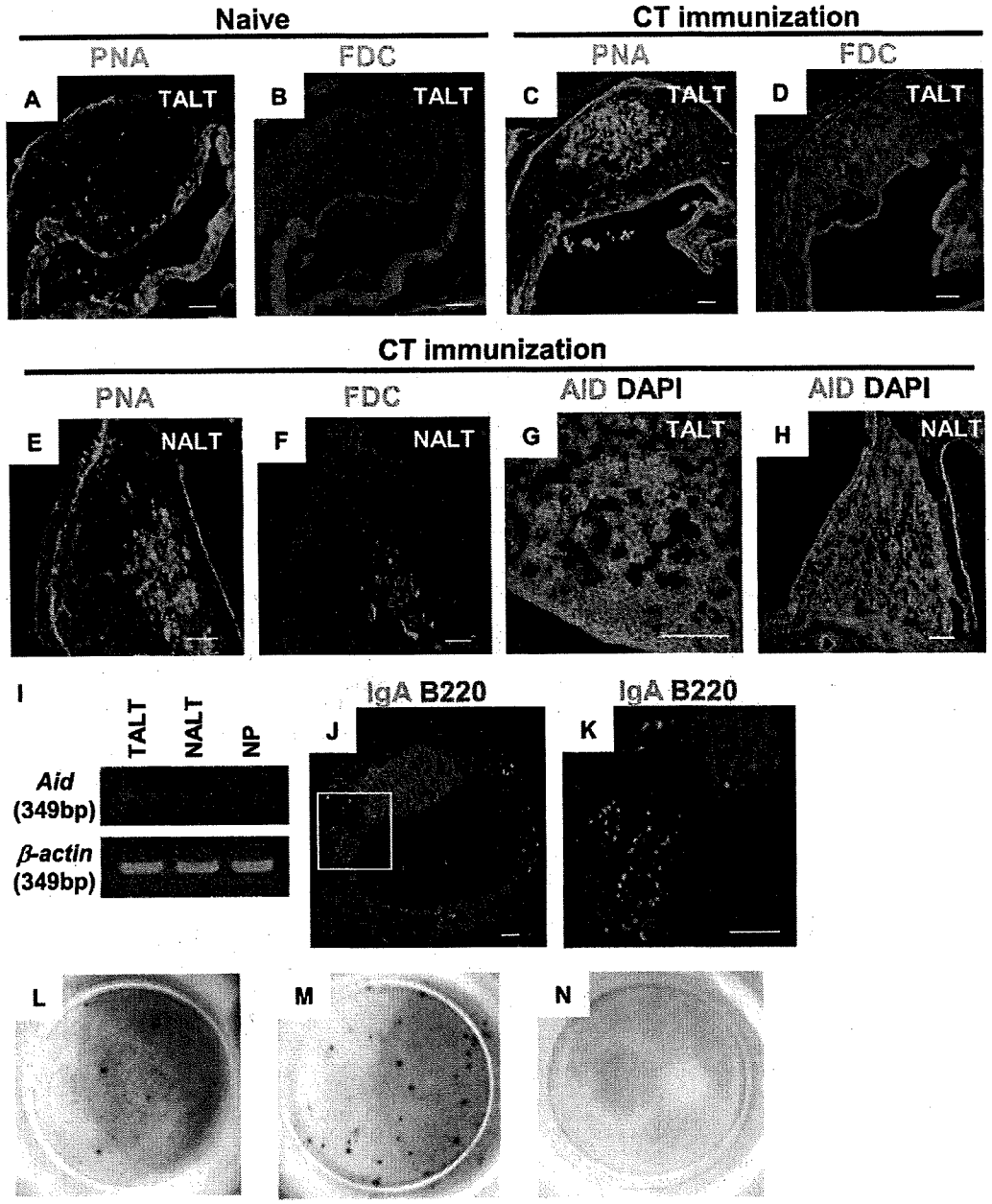

Figure 6. Induction of antigen-specific IgA responses through TALT. (A and B) Naive mice do not form GCs ($n = 3$ mice). (C and D) Mice were given CT by eye drops three times at 1-wk intervals. 1 wk after the last administration, TALT was isolated and examined with confocal microscopy. The CT challenge induced GC formation in TALT (C and D) and NALT (E and F; $n = 3$ mice/group). Tissues were stained with PNA (A, C, and E) or for FDCs (B, D, and F). (G and H) AID expression in TALT (G) and NALT (H) was detected in mice ocularly immunized with CT ($n = 3$ mice/group). (I) RT-PCR analysis of *Aid* expression in TALT, NALT, and NPs of mice given ocular CT ($n = 3$ mice/group). (J and K) Distribution of IgA^+B220^- plasma cells in tear ducts was examined with confocal microscopy. K is a magnified view of the box in J. CT challenge by eye drops induced the appearance of a large number of plasma cells in the tear duct compartment ($n = 3$ mice/group). (L–N) ELISPOT analysis for the detection of CT-B–specific IgA-producing cells in tear ducts (L) and CT-B–specific IgG-producing cells in spleens (M). Data obtained from control naive mice are shown in N. These data are representative of at least two independent experiments ($n = 4$ mice/group). Bars, 50 µm.

Published October 26, 2009

that TALT is the main gateway and inductive site for the initiation of antigen-specific T and B cell responses against ocularly encountered antigens. Collectively, these observations indicate that TALT is an important member of the MALT family. It has a lymphoid structure that is organized as an inductive site for antigen uptake and the initiation of antigen-specific mucosal immune responses with GC formation and Ig class switching, as well as the generation of antigen-specific CD4+ T cells.

DISCUSSION

Our purpose was to investigate the developmental features of TALT and to reveal the immunological importance of this tissue in immune surveillance for mucosal immunity. We found that the molecular requirements of TALT organogenesis were quite different from those of other secondary lymphoid organs. For example, the initiation of TALT organogenesis is independent of the IL-7R– and LTβR–NIK–mediated tissue genesis pathways, and thus, its structure was preserved in mice lacking other secondary lymphoid organs, such as *Il-7rα*$^{-/-}$, *Ltα*$^{-/-}$, and *aly/aly* mice (Table I). Furthermore, the TNF-related activation-induced cytokine (TRANCE)–mediated pathway, which is involved in pLN development (Kong et al., 1999), was dispensable for TALT genesis. Thus, the TALT structure was found in *Trance*$^{-/-}$ mice and in mice null for its signal transducer, TNF receptor–associated factor (TRAF) 6 (Fig. S5). However, these mice lacking secondary lymphoid organs (e.g., *Il-7rα*$^{-/-}$, *Ltα*$^{-/-}$, and *aly/aly* mice) had smaller TALT volumes than were found in WT mice. LTβR–NIK–mediated signals induce the production of lymphoid chemokines such as CXCL13, CCL19, and CCL21, and adhesion molecules, including VCAM-1 and PNAd (Dejardin et al., 2002; Browning et al., 2005). The immature formation of TALT in mice deficient in LTβR-associated molecules can therefore be explained by the lack of lymphoid chemokines and adhesion molecules involved in leukocyte migration. In support of this, the extent of the TALT in *Cxcl13*$^{-/-}$*plt/plt* mice was smaller than that in *Cxcl13*$^{-/-}$ and *plt/plt* single- or double-mutant mice, as well as in WT mice. However, accumulation of some B lymphocytes was seen in these mutant mice (Fig. S3). Thus, we cannot eliminate the possibility that the migration stage of B lymphocytes may also operate independently of the LTβR–NIK pathway for TALT genesis.

One of the important findings of our study is that TALT genesis occurs in both *Id2*$^{-/-}$ and *Rorγt*$^{-/-}$ mice. TALT genesis takes place normally in *Rorγt*$^{-/-}$ mice despite the fact that CD3$^-$CD4$^+$CD45$^+$ LTi cells, and as a consequence PPs and pLNs, are totally absent in these mice (Sun et al., 2000; Eberl et al., 2004). In addition, Id2 is the key transcriptional regulator for the induction and differentiation of CD3$^-$CD4$^+$CD45$^+$ LTi cells (Yokota et al., 1999). *Id2*$^{-/-}$ mice do not develop any form of secondary lymphoid tissues, including pLNs, PPs, or NALT (Yokota et al., 1999; Fukuyama et al., 2002). However, TALT development is Id2 and RORγt independent (Table I). We still found that CD3$^-$CD4$^+$CD45$^+$ cells, which we hypothesize to be TALT inducer cells, existed at TALT anlagen in both *Id2*$^{-/-}$ and *Rorγt*$^{-/-}$ mice, and we revealed that CD3$^-$CD4$^+$CD45$^+$ cells isolated from TALT anlagen did not express either *Id2* or *Rorγt*. A recent study showed that omental milky spots developed in the absence of LTi cells (Rangel-Moreno et al., 2009). Omental milky spots were found in *Id2*$^{-/-}$ and *Rorγt*$^{-/-}$ mice. However, this tissue development required the lymphoid chemokine CXCL13. Because the initiation of TALT development is independent of CXCL13, omental milky spots and TALT use different tissue

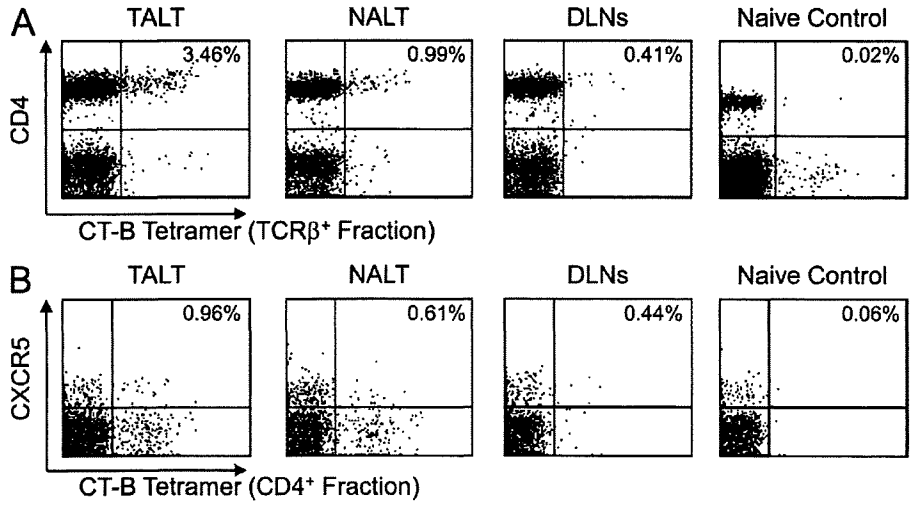

Figure 7. Induction of antigen-specific CD4+ T cell responses in TALT after ocular immunization. (A and B) FACS analysis of CT-B tetramer-positive cells in lymphocytes isolated from TALT, NALT, and draining LNs (DLNs; cervical and submandibular LNs) of CT-immunized or naive mice. Data from TCRβ+ (A) and CD4+ (B) populations are shown. TALT preferentially responded to ocular administration of CT and generated CT-B–specific CD4+ T cells, including CXCR5+ T follicular helper cells. These data are representative of at least two independent experiments (n = 4 mice/group).

Published October 26, 2009

Table I. Distinct molecular features for organogenesis of different MALTs

Mice	TALT	NALT	PP	CLN	MLN	ILF	Cryptopatch	References
Id2$^{-/-}$	+++	−	−	−	−	ND	ND	*1
Rorγt$^{-/-}$	+++	+++	−	−	−	−	+/−	*2
Ltα$^{-/-}$	+	+	−	−	+/−	−	+/−	*3
aly/aly	+	+	−	−	−	−	++	*4
Il-7rα$^{-/-}$	++	++	−	+/−	++	++	−	*5
Cxcl13$^{-/-}$	++	+	+/−	+/−	++	ND	ND	*6
plt/plt	+++	++	++	++	++	ND	ND	*7
Cxcl13$^{-/-}$*plt/plt*	+	+	+/−	−	++	ND	ND	*8

CLN, cervical LN; MLN, mesenteric LN. +++, developed well; ++, developed with decreased number of lymphocytes; +, developed with few number of lymphocytes; −, absent; +/−, present or absent, depends on individual. *1, Yokota et al., 1999; Fukuyama et al., 2002; Boos et al., 2007; *2, Sun et al., 2000; Harmsen et al., 2002; Eberl and Littman, 2004; Eberl et al., 2004; Naito et al., 2008; Tsuji et al., 2008; *3, De Togni et al., 1994; Banks et al., 1995; Suzuki et al., 2000; Fukuyama et al., 2002; Hamada et al., 2002; Harmsen et al., 2002; Taylor et al., 2004; *4, Kanamori et al., 1996; Shinkura et al., 1999; Fukuyama et al., 2002; Hamada et al., 2002; *5, Peschon et al., 1994; Kanamori et al., 1996; Adachi et al., 1998b; Fukuyama et al., 2002; Hamada et al., 2002; Luther et al., 2003; *6, Ansel et al., 2000; Rangel-Moreno et al., 2005; Fukuyama et al., 2006; *7, Nakano et al., 1997; Rangel-Moreno et al., 2005; Fukuyama et al., 2006; and *8, Luther et al., 2003; Rangel-Moreno et al., 2005; Fukuyama et al., 2006.

genesis mechanisms. The organogenesis of secondary lymphoid tissues has been shown to require several processes, including the trafficking/accumulation of LTi cells, the differentiation/activation of specialized stromal cells, and the trafficking/accumulation of conventional lymphocytes (Mebius, 2003). In this light, the genesis of these tissues can be separated into at least two phases, initiation and maturation; in other words, the migration of LTi cells and lymphocytes, respectively, to the tissue development site. Our results indicate that the initiation of TALT genesis operates independently of the requirement for the classical tissue genesis–associated signaling cascade of IL-7R/LTβR–NIK because leukocytes, including B lymphocyte, already migrated to TALT without this pathway. Further, the unique CD3$^-$CD4$^+$CD45$^+$ cells develop without a requirement for the LTi cell–associated transcriptional regulators Id2 and RORγt, and are identified as the first hematopoietic cell population that migrates to the TALT anlagen. To directly address the critical role of Id2- and RORγt-independent CD3$^-$CD4$^+$CD45$^+$ cells (or TALT inducer cells) in the initiation of TALT genesis, our efforts are now directed toward finding and/or developing TALT-deficient mice for the necessary adoptive transfer experiment.

TALT organogenesis occurs after birth, as does NALT genesis (Fukuyama et al., 2002). In contrast, PPs and pLNs are initially generated during the embryonic period (Mebius, 2003). These findings suggest that secondary lymphoid tissue genesis can be chronologically separated into two categories: a prenatal group (PPs and pLNs) and a postnatal group (TALT and NALT). However, initiation of genesis of all of these tissues, including TALT, occurs independently of microbial stimuli.

Ocular surface antigens are taken up by NALT, and NALT might function as an inductive site for tear IgA production (Ridley Lathers et al., 1998). However, our findings suggest that TALT is a key inductive tissue for immune responses, because TALT is a more important site for the generation of antigen-specific T cells than NALT and, thus, contributes to mucosal immune responses against ocularly encountered antigens. In support of this suggestion, our study showed the presence of a mucosal gateway population of M cells in TALT that is capable of taking up ocularly administered bacterial antigens (e.g., *Salmonella*). Ocular infection with *P. aeruginosa* causes corneal ulcers and sometimes loss of vision (Liesegang, 1998), and we found *P. aeruginosa* given by ocular challenge within TALT, leading to the subsequent formation of GCs. These findings indicate that TALT plays an important role in ocular immune surveillance and protection, providing the first line of defense of the host's eyesight; we can therefore expect it to be equivalent in its capacity for immunosurveillance to the other well-known mucosal inductive tissues in the aerodigestive tract, NALT and PPs.

The lacrimal glands are effector sites for IgA production because their tissue contains large numbers of IgA-producing cells (Sullivan and Allansmith, 1984; Peppard and Montgomery, 1987; Saitoh-Inagawa, 2000). We also found that a large number of IgA$^+$B220$^-$ plasma cells were distributed around the diffuse tissues of the NPs and in the tear duct in response to CT immunization via eye drops. Thus, TALT and various tissues of the tear duct are responsible for ocular immunity as inductive and effector sites, respectively.

In summary, our results demonstrated the presence of mouse TALT, providing the first definitive evidence for the existence of Id2-, RORγt-, and LTβR-independent lymphoid tissue genesis. In addition, TALT was shown to play an important role in the induction of antigen-specific immune responses and to function in immune surveillance in ocular immunity.

MATERIALS AND METHODS

Mice. C57BL/6 and BALB/c mice were purchased from Japan SLC; germ-free and *aly/aly* mice were purchased from CLEA Japan; and *Ltα*$^{-/-}$, *Igh6*$^{-/-}$, *Tcrβ*$^{-/-}$, and *Tcrδ*$^{-/-}$ mice were purchased from the Jackson Laboratory. *Il-7rα*$^{-/-}$ mice were provided by Immunex Corp., and were also purchased from the Jackson Laboratory. *Id2*$^{-/-}$, *Rorγt*$^{-/-}$, *Cxd13*$^{-/-}$, *Tlr2*$^{-/-}$, *Tlr4*$^{-/-}$, *MyD88*$^{-/-}$, *Cxd13*$^{-/-}$*plt/plt*, *Trance*$^{-/-}$, and *Traf6*$^{-/-}$ mice were generated as previously described (Adachi et al., 1998a; Hoshino et al., 1999; Kong et al., 1999; Naito et al., 1999; Takeuchi et al., 1999;